Lithosphere

Age and origin of granites in the Karakoram shear zone and Greater Himalaya Sequence, NW India

Forrest Horton and Mary L. Leech

Lithosphere published online 20 April 2013;
doi: 10.1130/L213.1

Notes

Lithosphere, published online on 20 April 2013 as doi:10.1130/L213.1

Age and origin of granites in the Karakoram shear zone and Greater Himalaya Sequence, NW India

Forrest Horton* and Mary L. Leech†
GEOSCIENCES DEPARTMENT, SAN FRANCISCO STATE UNIVERSITY, 1600 HOLLOWAY AVENUE, SAN FRANCISCO, CALIFORNIA 94132, USA

ABSTRACT

The crustal-scale Karakoram shear zone structurally distinguishes the western Himalaya from—and provides an opportunity to compare to—the central and eastern portions of the orogen. To evaluate the tectonic evolution of the western Himalaya, this paper presents granite U/Th-Pb ages and zircon Hf isotopic signatures along the two major structures in northern India: the Karakoram shear zone and the Zanskar shear zone, the westernmost limb of the South Tibetan detachment system. Leucogranites in Zanskar crystallized 27–20 Ma and exhibit Precambrian to Paleozoic inheritance and predominantly negative $\varepsilon_{Hf}(t)$ values typical of the Greater Himalayan Sequence. Karakoram shear zone leucogranites have igneous crystallization ages over a prolonged period from 22 Ma to <13 Ma, contain Late Cretaceous through Paleocene inherited cores, and have $\varepsilon_{Hf}(t)$ values from +1 to +9. These inherited ages and mostly positive $\varepsilon_{Hf}(t)$ values compare closely to the adjacent Ladakh batholith, but low $\varepsilon_{Hf}(t)$ values along the Karakoram shear zone suggest an input of older crustal material from the proximal Karakoram terrane or subducted Indian crust. The Zanskar Greater Himalayan Sequence contains two suites of Paleozoic granites: (1) Pan-African Cambrian–Ordovician granites at the cores of gneiss domes and (2) Mississippian–Permian granites related to magmatism associated with the Panjal Traps. Monazite ages record peak through retrograde metamorphic conditions from 27.3 ± 1.2 Ma to 17.2 ± 0.9 Ma concurrent with anatectic leucogranite crystallization. Cenozoic partial melting in the Greater Himalayan Sequence occurred contemporaneously across the Himalayan orogen, but lower degrees of partial melting and ubiquitous doming distinguish the westernmost Greater Himalayan Sequence in Zanskar.

LITHOSPHERE GSA Data Repository Item 2013173 doi: 10.1130/L213.1

INTRODUCTION

The Himalayan orogen is the largest active continental collision zone in the world with consistent tectonic structure for ~2500 km (Yin and Harrison, 2000) and the best natural laboratory for studying collisional tectonics. Consequently, orogenic models developed for the Himalaya are the foundation for understanding orogenies around the world (e.g., the Appalachians, Canadian Cordillera, and Hellenides); such models also demonstrate a link between tectonic and climatic processes (e.g., Whipple, 2009). Large-scale crustal shortening and extrusion along the Himalayan orogen have been explained by a midcrustal channel flow model (e.g., Nelson et al., 1996; Grujic et al., 2002; Beaumont et al., 2004; Godin et al., 2006; Grujic, 2006), in which subducting Indian crust undergoes partial melting beneath a thickened Tibetan Plateau and is gravitationally driven southward as a ductile channel to the southern Himalayan range front, where monsoonal precipitation causes rapid erosion (Beaumont et al., 2004). Proponents of the channel flow model correlate bright spots on seismic-reflection profiles and magnetotelluric data from the eastern Himalaya that show the presence of partial melts and a conductive layer in the middle crust to the southward extrusion of migmatites and leucogranites (Nelson et al., 1996; Grujic et al., 2002; Unsworth et al., 2005).

The 1000-km-long crustal-scale Karakoram shear zone—potentially responsible for hundreds of kilometers of lateral offset—distinguishes the western Himalaya from the central and eastern Himalaya. In northwest India, migmatites and related Miocene granites are prevalent along the Karakoram shear zone and along the westernmost limb of the South Tibetan detachment system; understanding the granite magmatism along these major structures is critical for evaluating the tectonic evolution of the western Himalaya. This paper presents geochronologic analysis and isotopic characterization of granites from two field areas: the Pangong Mountains along the Karakoram shear zone and the Zanskar valley along the Zanskar shear zone.

GEOLOGIC BACKGROUND

Karakoram Shear Zone

The dextral Karakoram shear zone extends southeast ~1000 km from the Pamir range near the Nanga Parbat syntaxis to the Ayilari area and the Gurla Mandhata detachment system in the Himalaya, broadly separating the Qiangtang and Lhasa terranes in the northeast from the Karakoram terrane, the Ladakh batholith, and Indian Himalayan units in the southwest (Fig. 1). The Karakoram shear zone has been interpreted as a crustal-scale fault (Rolland and Pêcher, 2001; Murphy et al., 2002), initializing after 15 Ma with an offset of 35–150 km (Murphy et al., 2002; Bhutani et al., 2003; Searle and Phillips, 2007), or prior to ca. 22 Ma with a total offset of >200 km (Lacassin et al., 2004; Valli et al., 2007, 2008; Boutonnet et al., 2012). Right-lateral offsets of late Pleistocene glacial moraines indicate slip rates of ~10 mm/yr (Chevalier et al., 2005a), but global positioning system (GPS) measurements along the Karakoram shear zone indicate a significantly lower contemporary slip rate of 3–4 mm/yr (Jade et al., 2004), which is supported by recent correlation of offset markers indicating 4.5 mm/yr in the Ayilari range (Wang et al., 2012). Whether earthquake rupture or gradual fault creep is the dominant slip mechanism along the Karakoram shear zone is currently unresolved (see discussion in Brown et al., 2005; Chevalier et al., 2005b). Recent studies have discussed the possibility that the Karakoram shear zone has interacted with underlying partially melted Indian crust (Leech,

*Current address: Earth Science Department, University of California–Santa Barbara, 1006 Webb Hall, Santa Barbara, California 93106, USA; fhorton@umail.ucsb.edu.
†E-mail: leech@sfsu.edu

Lithosphere, published online on 20 April 2013 as doi:10.1130/L213.1

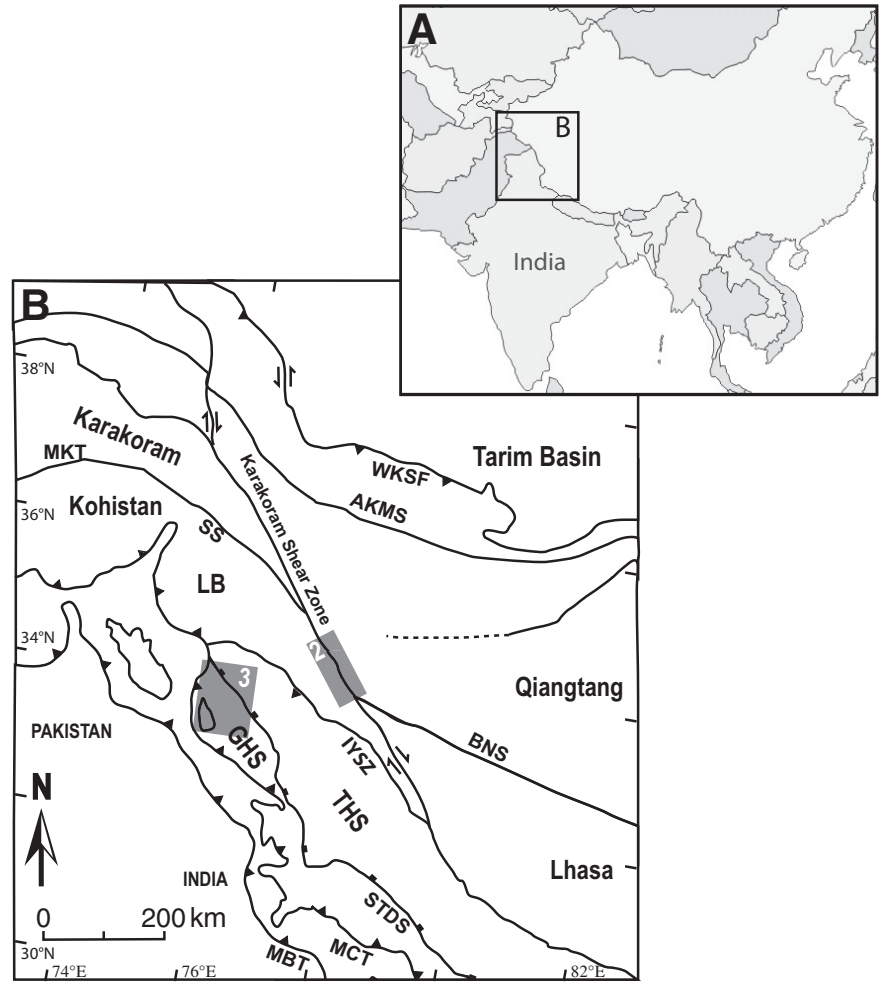

Figure 1. Regional maps (A) showing national boundaries, and (B) showing major lithotectonic and structural boundaries and field locations, modified from Phillips (2008). Shaded rectangles show the location of Figures 2 and 3. Abbreviations: AKMS—Ayimaqin-Kunlun-Muztagh suture, BNS—Bangong-Nujiang suture, GHS—Greater Himalaya Sequence, IYSZ—Indus-Yarlung suture zone, LB—Ladakh batholith, MBT—Main Boundary thrust, MCT—Main Central thrust, MKT—Main Karakoram thrust, SS—Shyok suture, STDS—South Tibetan detachment system, THS—Tethyan Himalaya Sequence, WKSF—Western Kunlun Shan fault.

2008; Ravikant et al., 2009; Leloup et al., 2011), potentially impeding southward extrusion of middle crust in the western Himalaya, and $^{3}He/^{4}He$ ratios from geothermal springs along the Karakoram shear zone demonstrate that the fault penetrates to Tibetan mantle, acting as a northern backstop to subducted Indian crust and channel flow (Klemperer et al., 2013).

In northern India, the Karakoram shear zone separates the Karakoram terrane in the north from the Ladakh batholith (generally considered equivalent to the Kohistan arc in Pakistan and related in origin to the Gangdese batholith to the east) and associated Kardung volcanics in the south (Fig. 2). Ladakh batholith granites were emplaced during Cretaceous (103–83 Ma) and early Cenozoic (67–50 Ma) arc magmatism associated with the subduction of the Neotethys oceanic crust (e.g., Dunlap and Wysoczanski, 2002; Ravikant et al., 2009). The Karakoram terrane contains metasedimentary and granitic rock with ages from 130 to 35 Ma and a primary magmatic episode at ca. 105 Ma that produced Hunza granodiorite (Fraser et al., 2001; Heuberger et al., 2007). Inherited zircons from the granodiorite yielded ages of ca. 1850 Ma (Heuberger et al., 2007), suggesting Karakoram terrane granites may have been derived from Gondwanan crust.

In the Pangong Tso area (Fig. 2), the Karakoram shear zone has a left step and splays into two strands, with the northern Pangong strand running along the Shyok valley and Pangong Tso. The southern Tangste strand cuts through Darbuk and Tangste villages (Searle et al., 1998). Between the two strands, multiple generations of anatectic leucogranites and upper-amphibolite-facies metapelites and metagranulites indicate metamorphism at >800 °C (Rolland and Pêcher, 2001). Weinberg et al. (2009) proposed that transcurrent fault motion facilitated the accumulation of anatectic melts and that subsequent transpression and uplift led to the exhumation of the entire sequence of amphibolites, migmatites, and leucogranites. The northern Tangste gorge contains migmatites that fed small plutons (Weinberg and Mark, 2008), whereas the southern Tangste gorge exposes primarily calc-alkaline amphibolites intruded by two-mica leucogranites (Phillips et al., 2004). Previous studies report leucogranite ages from 25 to 13 Ma (e.g., Searle et al., 1998; Phillips et al., 2004; Ravikant et al., 2009; Reichardt et al., 2010; Boutonnet et al., 2012). To the northwest, the Karakoram shear zone extends through Nubra valley as a single strand containing leucogranites coeval with those in Tangste Gorge (Jain and Singh, 2008; Phillips, 2008).

Greater Himalaya Sequence in Zanskar

The Greater Himalayan Sequence is composed of high-grade metasedimentary rocks and orthogneiss that are separated from the underlying lower-grade Lesser Himalaya Sequence by the Main Central thrust. The Greater Himalayan Sequence is bounded in the north by the South Tibetan detachment system and the overlying sedimentary Tethyan Himalaya Sequence (Fig. 3). The westernmost limb of the Greater Himalayan Sequence extends into the Zanskar region of northwest India, composed of the Zanskar, Doda, and—for purposes of this paper—the Suru River watersheds (Fig. 1). In Zanskar, the Greater Himalayan Sequence contains Precambrian metapelites, migmatites, Paleozoic granites, and Miocene anatectic granites (Honegger et al., 1982; Honegger, 1983; Herren, 1987b) that are collectively separated from overlying Tethyan sediments by the extensional Zanskar shear zone, the western equivalent of the South Tibetan detachment system (Fig. 3). Zanskar contains Cambrian–Ordovician granite intrusions (Frank et al., 1977; Mehta, 1977; Stutz and Thöni, 1987; Pognante et al., 1990; Noble and Searle, 1995; Walker et al., 1999), as well as several small bodies of Permian granite (Honegger et al., 1982; Spring et al., 1993; Noble et al., 2001). Igneous monazite ages for Miocene granites have only been obtained near Gumberanjun in SE Zanskar (Dézes et al., 1999; Walker et al., 1999) and in Nun-Kun valley (Noble and Searle, 1995). Miocene granites farther northwest in the Nanga Parbat massif are geochemically dissimilar and may be derived from Tethyan Himalaya Sequence metasediments (Whittington et al., 2000).

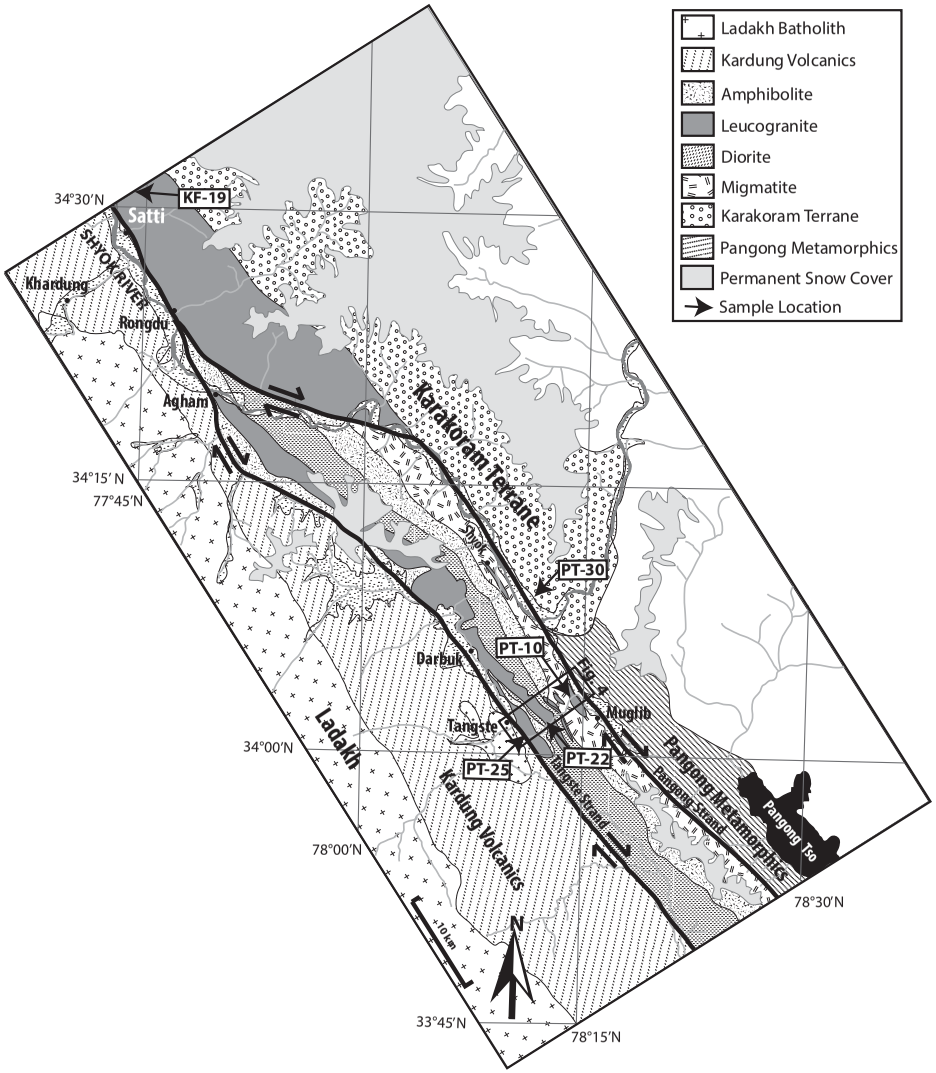

Figure 2. Map of part of the Karakoram shear zone showing sample locations in the Tangste area, modified from Phillips (2008). The rectangle shows the location of Tangste gorge in Figure 4.

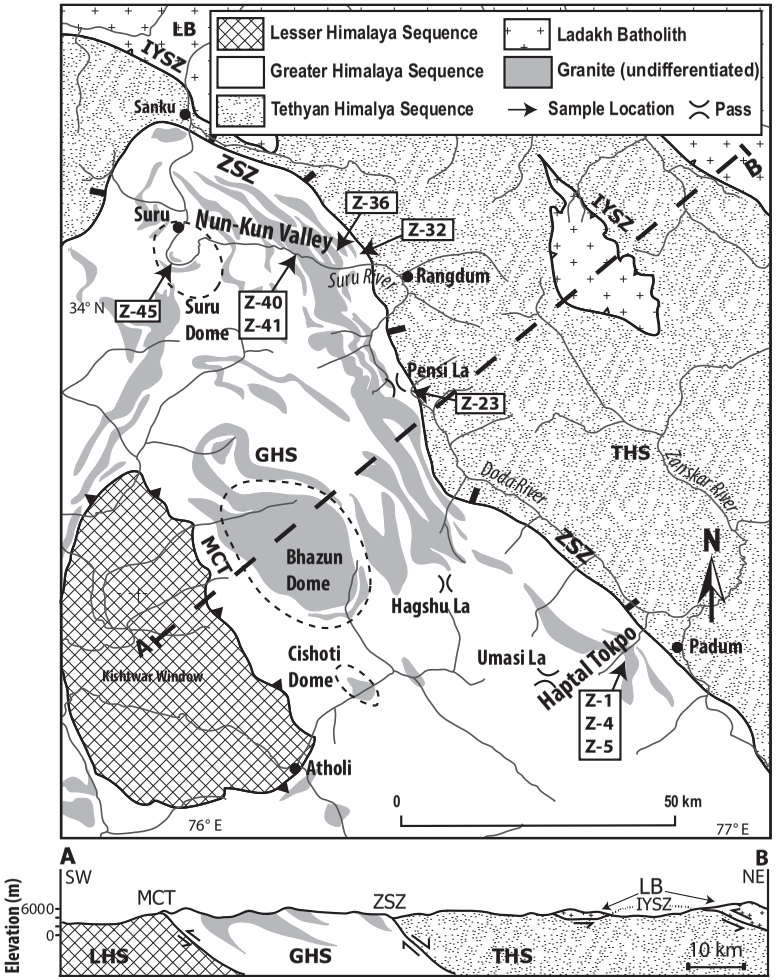

Figure 3. Geologic map of the Zanskar area showing sample locations, modified from Steck (2003), including a cross section based on Kundig (1989). The cross section demonstrates how the Greater Himalaya Sequence (GHS) is bounded by the Zanskar shear zone (ZSZ) to the northeast and by the Main Central thrust (MCT) to the southwest. See Figure 1 for location and complete list of abbreviations.

Lithosphere, published online on 20 April 2013 as doi:10.1130/L213.1

Barrovian metamorphism (M1) associated with the Himalayan orogeny lasted from ca. 40 Ma to 25 Ma (Searle et al., 1999; Vance and Harris, 1999), reaching peak kyanite-grade conditions between 33 Ma and 27 Ma at conditions of ~1.0 GPa and 620–650 °C (Walker et al., 2001). Top-to-the-SE shear sense and kilometer-scale folds in northwest Zanskar record the prograde compression and burial of the Greater Himalayan Sequence (Honegger et al., 1982). M1 isograds are telescoped along the Zanskar shear zone by a second stage of metamorphism (M2) that began with the activation of the Main Central thrust and Zanskar shear zone (Searle, 1986; Herren, 1987a; Searle and Rex, 1989). M2 metamorphism reached sillimanite-grade conditions of 0.45–0.7 GPa and 650–770 °C (Searle et al., 1999) that peaked when anatectic melting in upper levels of the Greater Himalayan Sequence began at 22–19 Ma (Noble and Searle, 1995; Dézes et al., 1999; Walker et al., 1999). Muscovite $^{40}Ar/^{39}Ar$ ages from Miocene leucogranites and nearby metasediments are ca. 20 Ma, suggesting rapid exhumation of the upper Greater Himalayan Sequence during or immediately after the M2 metamorphism (Walker et al., 1999; Dézes et al., 1999). During Miocene crustal shortening, the Zanskar Greater Himalayan Sequence developed a semicontinuous orogen-parallel series of domal structures extending from the Gumberanjun dome in the southeast through Cishoti, Haptal, Umasi La, Bhazun, and Suru domes to the northwest (Fig. 3; Herren, 1987b; Kundig, 1989; Searle et al., 1999).

Extension along the Zanskar shear zone began shortly before 26 Ma (Robyr et al., 2006) and continued until at least 17 Ma (Leloup et al., 2010, and references therein). Net displacement along the Zanskar shear zone has been estimated to be 25 km by Herren (1987a) and 35 ± 9 km by Dézes et al. (1999), but the absence of a major ductile shear zone northwest of Pensi La (Kundig, 1989) suggests that total offset decreases to the northwest in Zanskar. Slip estimates for the Zanskar shear zone account for the discrepancy in metamorphic grade between the Greater Himalayan Sequence (burial depths constrained to ≤40 km; Walker et al., 2001) and low-grade Tethyan Himalaya Sequence.

METHODS

Zircon U-Pb geochronology and trace-element analyses, as well as monazite Th-Pb geochronology analyses were conducted on the Stanford–U.S. Geological Survey sensitive high-resolution ion microprobe–reverse geometry (SHRIMP-RG) spectrometer at Stanford University. The high spatial resolution achievable with the SHRIMP allowed us to target zircon rims from the most recent crystallization event. Monazite ages were obtained to avoid problems associated with the high uranium concentrations common for Himalayan zircons and for instances in which zircon rims were too thin to target. Incorporation of ^{230}Th during monazite growth causes excess ^{206}Pb and disequilibrium in the U decay series, particularly in young monazites (Schärer, 1984; Parrish, 1990); the Th-Pb system is unaffected by this disequilibrium, and therefore we report the $^{232}Th/^{208}Pb$ ages as the most reliable ages for these monazites.

Additional zircon U-Pb geochronology and Lu-Hf isotopic analyses were done by multi-collector laser ablation–inductively coupled plasma–mass spectrometry (LA-ICP-MS) at the Arizona LaserChron Center at the University of Arizona (see Appendix A for method details).

RESULTS AND INTERPRETATION

Five samples from the Karakoram shear zone and nine samples from the Greater Himalayan Sequence in the Zanskar region were analyzed for U/Th-Pb geochronology data, trace elements, and Hf isotopes by SHRIMP and LA-ICP-MS analysis (see GSA Data Repository for data sets[1]). Samples were selected to represent the major granitic bodies and the geographical distribution of granites in each field area: Three Karakoram shear zone samples are from the Pangong range and are distributed between the Pangong and Tangste strands of the Karakoram shear zone, one is from the Karakoram terrane along the Pangong strand of the Karakoram shear zone, and one sample is from the Nubra valley area (Fig. 2); Zanskar samples are distributed NW-SE along the Zanskar shear zone from the Suru valley to Pensi La and to Haptal Tokpo near Padum (Fig. 3). SHRIMP analyses of zircon were conducted to acquire a suite of trace-element data; U/Th-Pb data for monazite were also collected using the SHRIMP. U-Pb and Hf isotope data were collected for the same zircon ablation spots by LA-ICP-MS. SHRIMP ages are ^{207}Pb-corrected $^{238}U/^{206}Pb$ ages unless otherwise noted, and LA-ICP-MS results are $^{238}U/^{206}Pb$ ages. The $^{238}U/^{206}Pb$ and $^{232}Th/^{208}Pb$ ages are presented for monazites, but $^{232}Th/^{208}Pb$ ages are preferred due to the incorporation of ^{230}Th (a partial decay product of ^{238}U) in monazite that causes apparent common Pb. Dating is summarized in Table 1; all

TABLE 1. SUMMARY OF LA-ICP-MS AND SHRIMP AGES

Sample	Rock type	Location		Mineral*	No. grains	Age populations (Ma)†
		Latitude (N°)	Longitude (°E)			
Karakoram shear zone						
PT-10	Syntectonic leucogranite dike	34°03′38.95″	78°13′52.61″	Zrn	30	21–13; 11.4 ± 0.2; 9.0 ± 0.2
PT-22	Deformed two-mica leucogranite	34°02′13.59″	78°12′41.79″	Zrn	21	65–38; 22.2–18.4
PT-25	Quartzofeldspathic mylonite	34°01′32.81″	78°10′34.90″	Zrn	25	85.7 ± 1.4; 22.8–16.6
PT-30	Nondeformed leucogranite dike	34°09′10.58″	78°11′08.41”	Zrn	23	157 ± 3
KF-19	Nondeformed leucogranite dike	34°37′59.02″	77°38′11.00″	Zrn	10	25.7–14.0
Zanskar Greater Himalayan Sequence						
Z-1	Migmatite	33°26′35.99″	76°46′35.51″	Mnz	26	21.5 ± 1.0
Z-4	Foliated leucogranite pluton	33°27′04.21″	76°46′06.49″	Mnz	10	461 ± 21
				Zrn	34	475–410; 27.2 ± 0.2; 21.6 ± 0.1
Z-5	Leucogranite pegmatite dike	33°27′04.21″	76°46′06.49″	Mnz	27	20.3 ± 1.7
Z-23	Granite	33°51′13.50″	76°22′39.11″	Mnz	15	436 ± 25
				Zrn	24	895–712
Z-32	Garnet schist	34°03′14.11″	76°17′34.33″	Zrn	11	1100–995
Z-36	Foliated leucogranite sill	34°03′01.44″	76°16′15.49″	Zrn	33	804 ± 27
Z-40	Schist	34°03′01.08″	76°14′41.17″	Mnz	20	27.3 ± 1.2
Z-41	Deformed leucogranite pluton	34°04′24.24″	76°10′29.99″	Zrn	28	360–264
Z-45	Deformed granite	34°03′41.65″	75°56′03.91″	Mnz	20	17.2 ± 0.9
				Zrn	33	284 ± 4.4; 47–25

Note: LA-ICP-MS—laser ablation–inductively coupled plasma–mass spectrometry; SHRIMP—sensitive high-resolution ion microprobe.
*Mnz—monazite; Zrn—zircon.
†$^{238}U/^{206}Pb$ age for zircon; $^{232}Th/^{208}Pb$ age for monazite.

[1]GSA Data Repository Item 2013173, Cathodoluminescence images, data tables, and color figures, is available at www.geosociety.org/pubs/ft2013.htm, or on request from editing@geosociety.org, Documents Secretary, GSA, P.O. Box 9140, Boulder, CO 80301-9140, USA.

U-Pb and cathodoluminescence imaging results for zircon are included in the Data Repository (see text footnote 1).

Karakoram Shear Zone—Tangste Gorge and Nubra Valley Areas

PT-10: Syntectonic Leucogranite Dike

This syntectonic leucogranite sample was collected near the Pangong strand of the Karakoram shear zone (Figs. 2 and 4) on the southern edge of the Tangste pluton (Fig. 5A). Bands of muscovite define irregular foliation in a strained quartz and feldspar matrix. Adjacent migmatite melanosomes consist of biotite psammite, and leucogranite dikes are less abundant farther from the main leucogranite body. Sector-zoned, euhedral PT-10 zircons (Fig. DR1 [see footnote 1]) provided 28 concordant SHRIMP ages (Fig. 6A). PT-10 yielded a broad range of Miocene ages, with most from 21 to <13 Ma, and two concordant analyses at 11.4 ± 0.2 Ma and 9.0 ± 0.2 Ma. LA-ICP-MS analysis of PT-10 zircon cores provided a tighter cluster of 16 spot ages at 17.4 ± 0.2 Ma and a single concordant inherited age of 69 ± 3 Ma (Fig. 6B). The lack of a pronounced negative Eu anomaly (Fig. 7A) for all Miocene SHRIMP analyses suggests that plagioclase was not growing during zircon crystallization. Older PT-10 spot analyses yielded higher Ce anomalies and higher light rare earth element (LREE) abundances. U/Ce ratios plotted against Th suggest that PT-10 zircons crystallized under anatectic melting conditions (Fig. 8A; Castiñeiras et al., 2010). Younger ages correspond to higher Hf concentrations and Yb/Gd ratios (Figs. 8C and 8D), probably caused by fractionation during cooling (see Barth and Wooden, 2010).

PT-22: Deformed Two-Mica Leucogranite

PT-22 is from a deformed two-mica leucogranite body in the central part of Tangste gorge (Figs. 2 and 4) with near-vertical contacts that crosscut adjacent leucogranite sheets intruded into dark psammite and calc-silicate (Fig. 5B). Elongated muscovite, biotite, quartz, and feldspar form the foliation, and there is accessory garnet. Zircon rims are predominantly Miocene, showing an even distribution of 12 SHRIMP ages ranging from 22.2 Ma to 18.4 Ma (Fig. 6C). Twenty-seven inherited oscillatory-zoned cores have LA-ICP-MS and SHRIMP ages from 65 Ma to 38 Ma (Fig. 6D); this age range may reflect mixing between core and rim domains. Trace-element data for PT-22 appear to be age dependent, with inherited Paleogene cores exhibiting greater negative Eu anomalies and less enrichment of heavy (H) REEs (as seen by lower Yb/Gd ratios) compared to Miocene rims (Fig. 7B). U/Ce versus

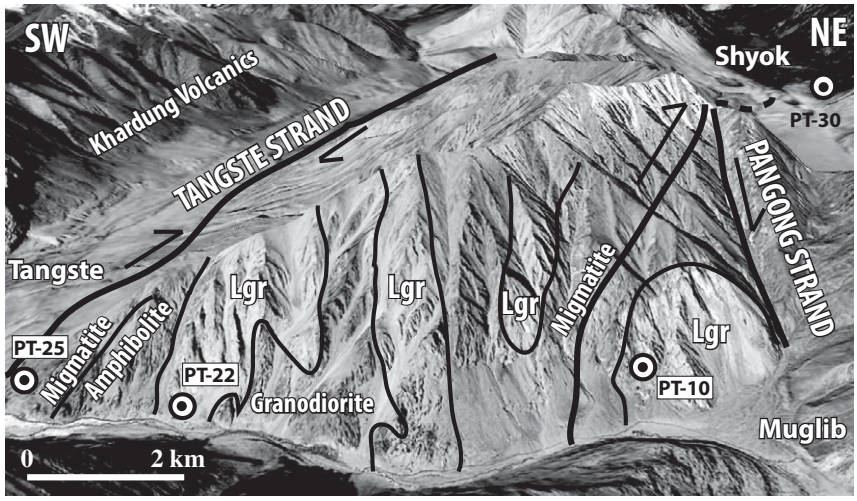

Figure 4. Annotated oblique satellite imagery of Tangste Gorge along the Karakoram shear zone showing sample locations (see Fig. 2 for location). Satellite imagery is from Google Earth and is presented at an inclined angle with no vertical exaggeration. Contacts and lithologies are based on field observations and Phillips and Searle (2007). Lgr—Leucogranite.

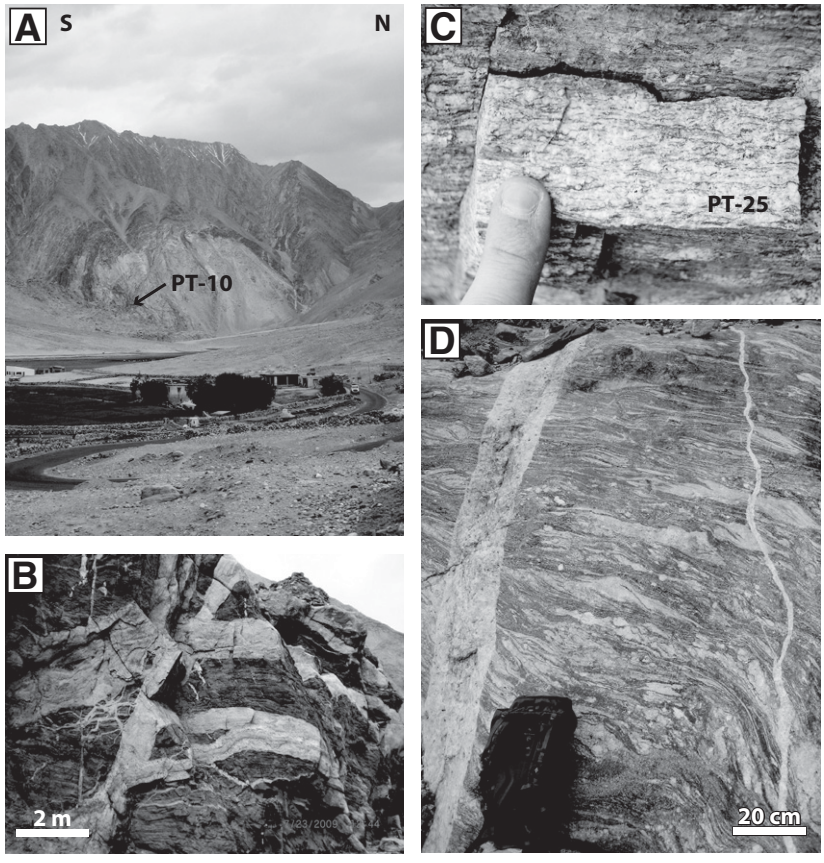

Figure 5. Field photographs from Pangong field area. (A) View of the Tangste pluton (sample PT-10) looking west from the village of Muglib along the Pangong strand of the Karakoram shear zone. Migmatized psammite foliation wraps around ponded leucogranite melt. (B) Leucogranite dikes intruded into Pangong amphibolite along the southern section of Tangste gorge. (C) Mylonitized leucogranite from the Tangste strand of the Karakoram fault near Tangste Gompa, with sigma clasts of feldspar showing shear sense (sample PT-25). (D) Mylonite from the Pangong strand of the Karakoram fault southwest of the Tangste pluton, crosscut by leucogranite dikes. The Data Repository contains a color version of this figure (see text footnote 1).

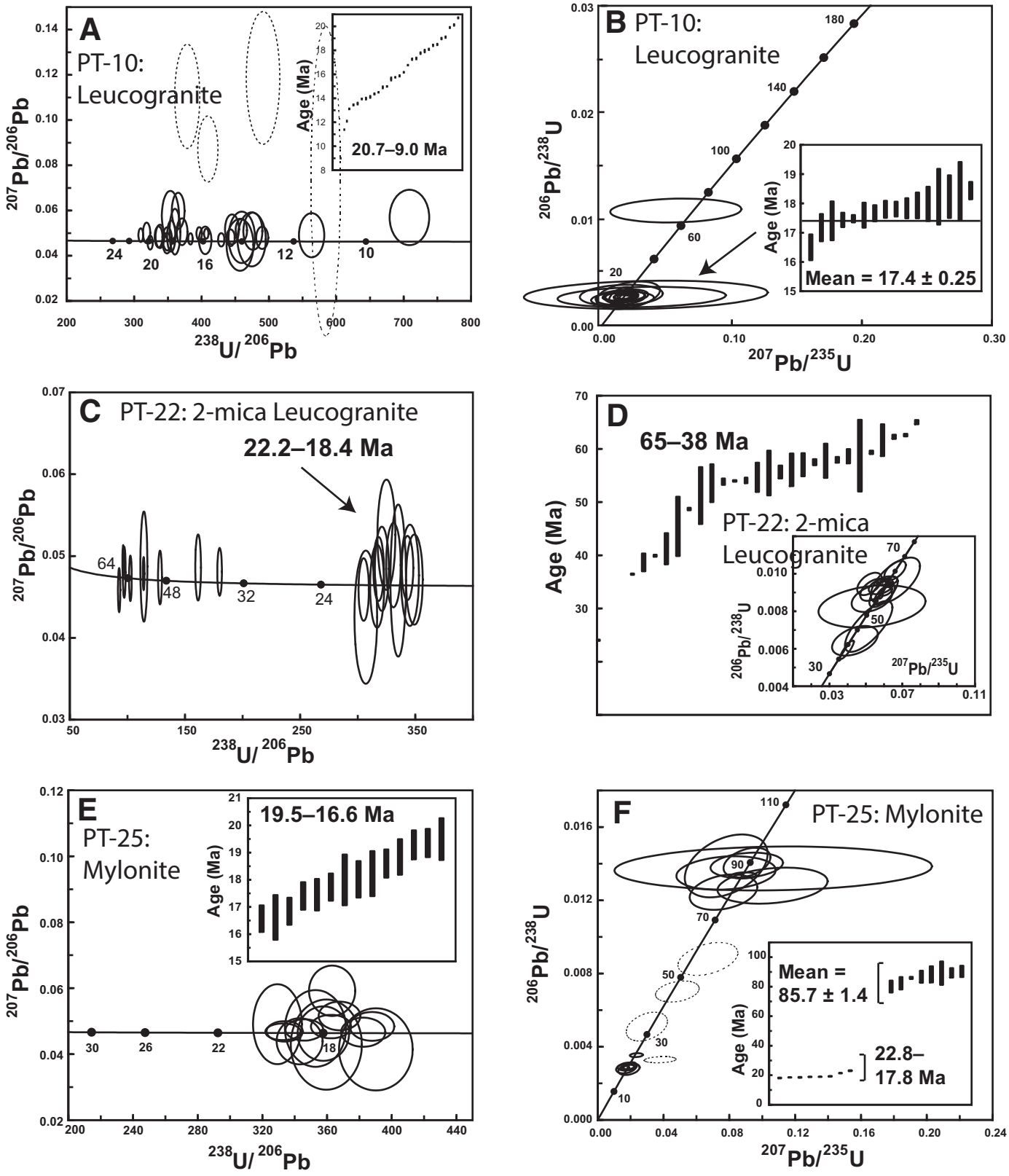

Figure 6. Concordia diagrams showing U-Pb sensitive high-resolution ion microprobe (SHRIMP) and laser ablation–inductively coupled plasma–mass spectrometry (LA-ICP-MS) data. Probability density plots show age distributions; means are presented for distinct age populations, and intercept lines are shown to assess mixing between zircon age domains. Mean ages are calculated from combined $^{206}Pb/^{238}U$ LA-ICP-MS ages and ^{207}Pb-corrected $^{206}Pb/^{238}U$ SHRIMP ages for samples analyzed with both methods. Dashed ellipses were not included in the calculated mean. ICP-MS data are included in B, D, F, I, L, and Q; other U-Pb diagrams are SHRIMP data.

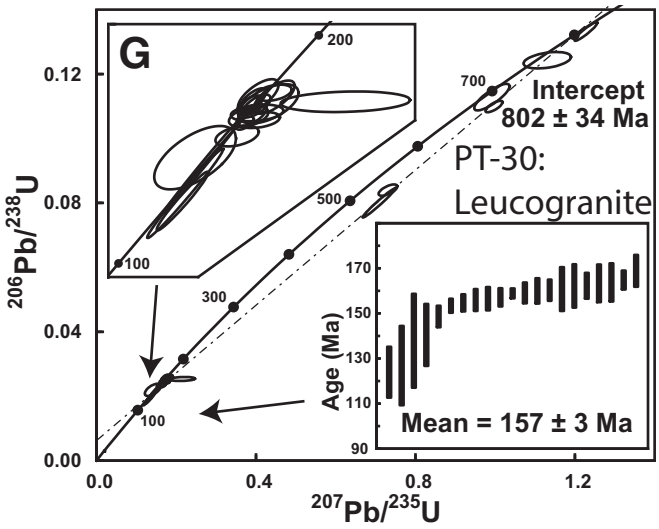

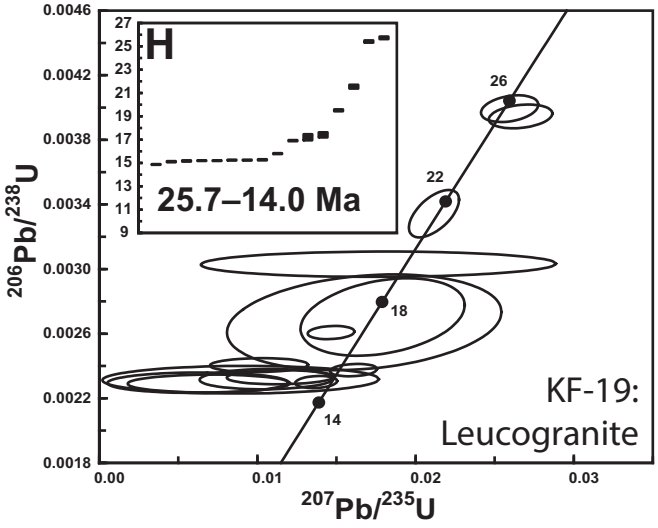

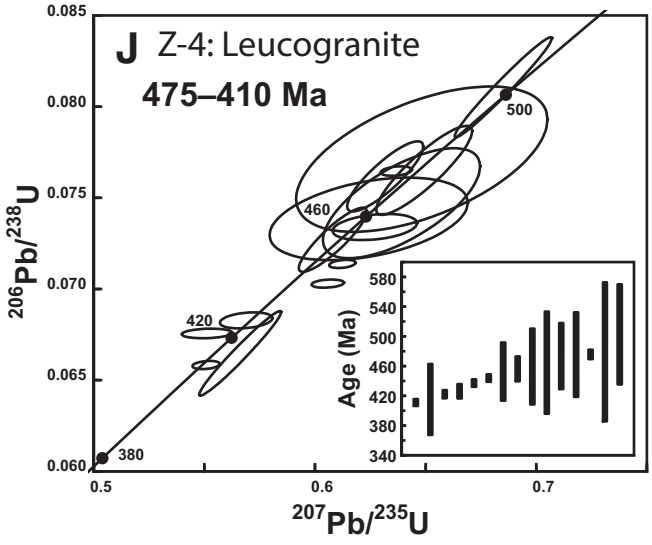

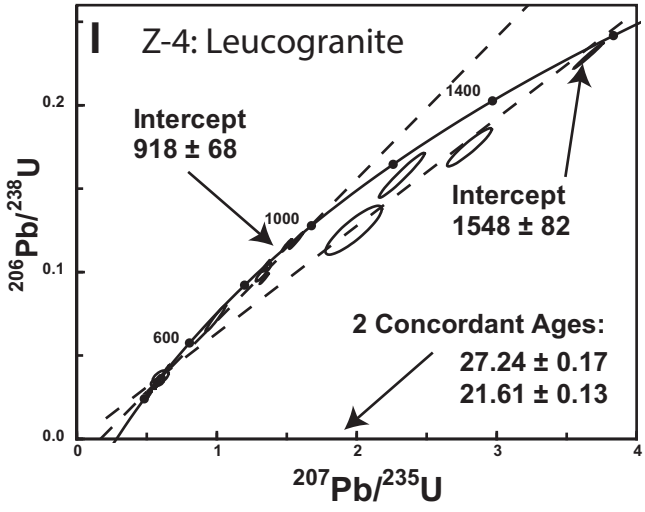

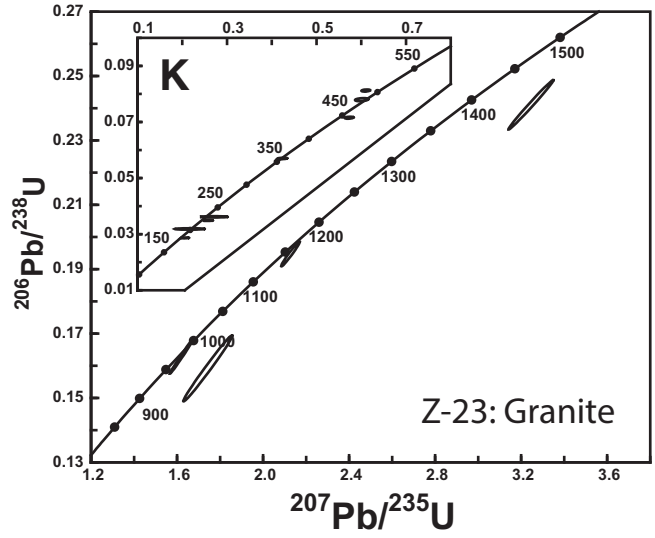

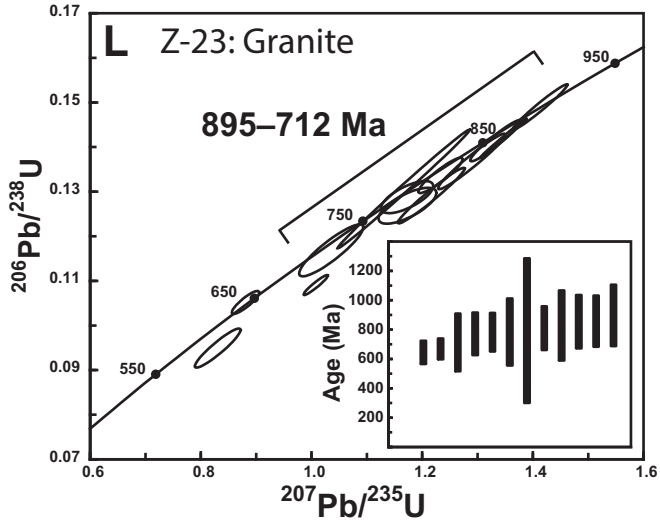

Figure 6 (*continued*).

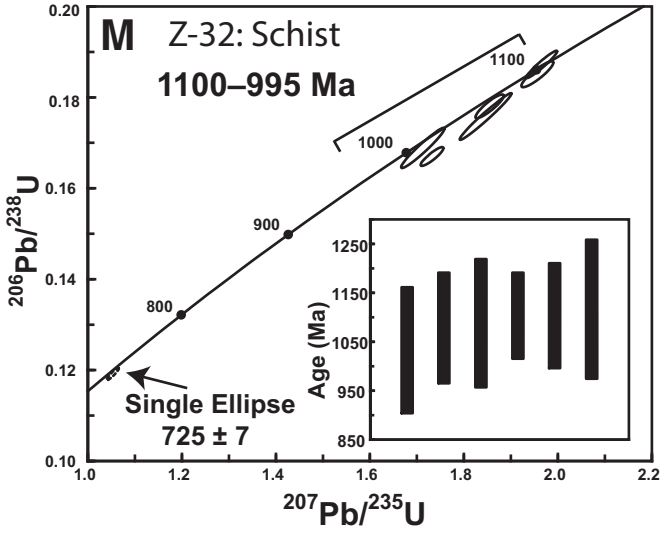

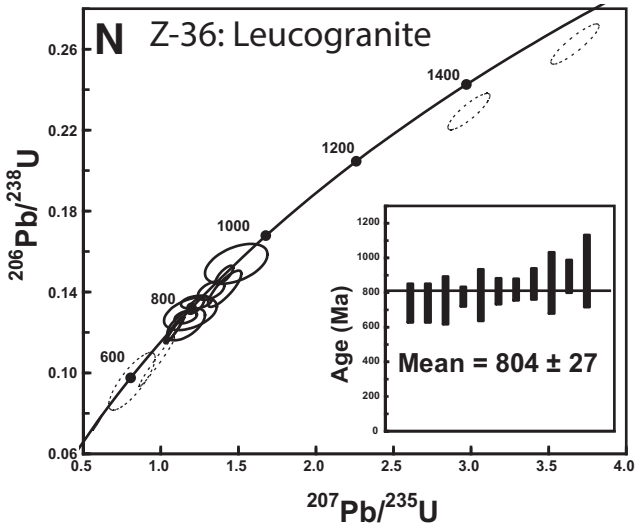

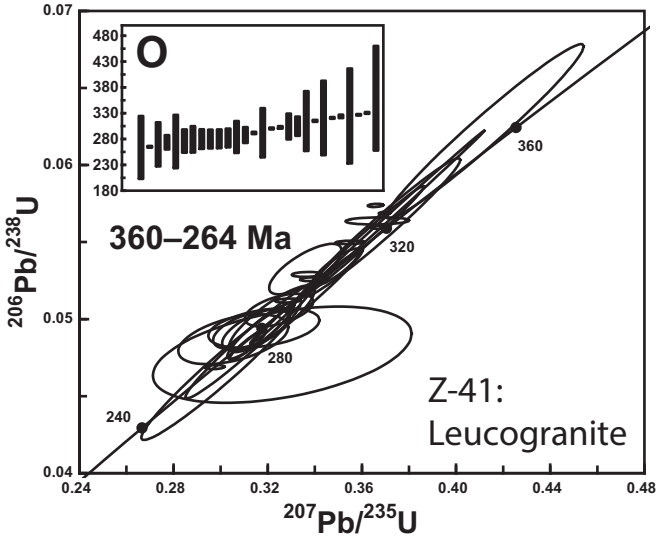

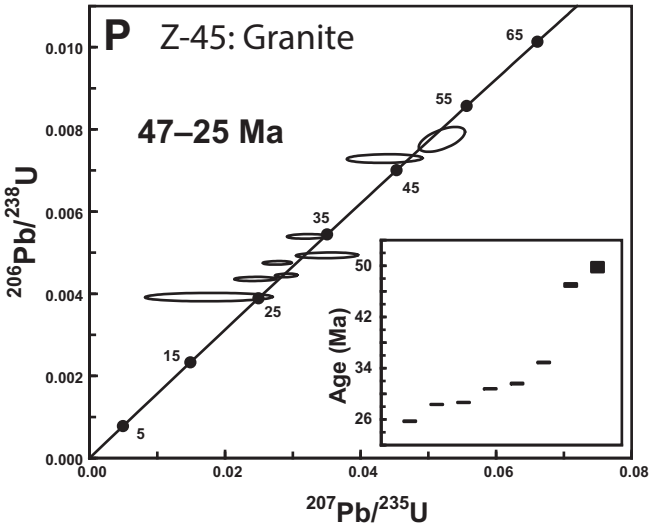

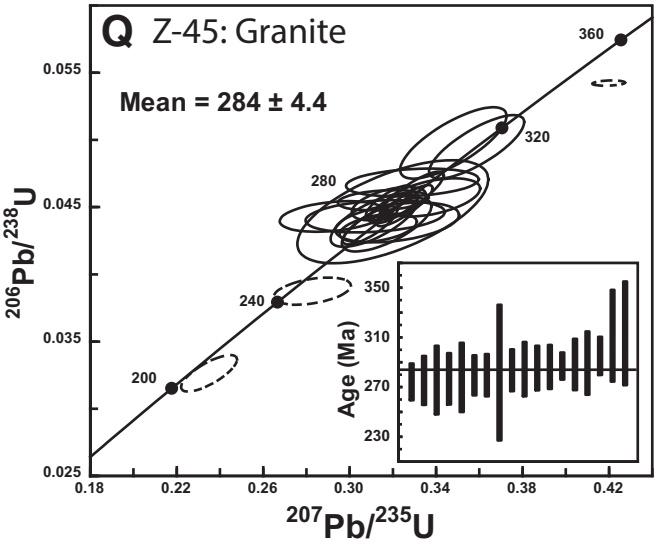

Figure 6 (*continued*).

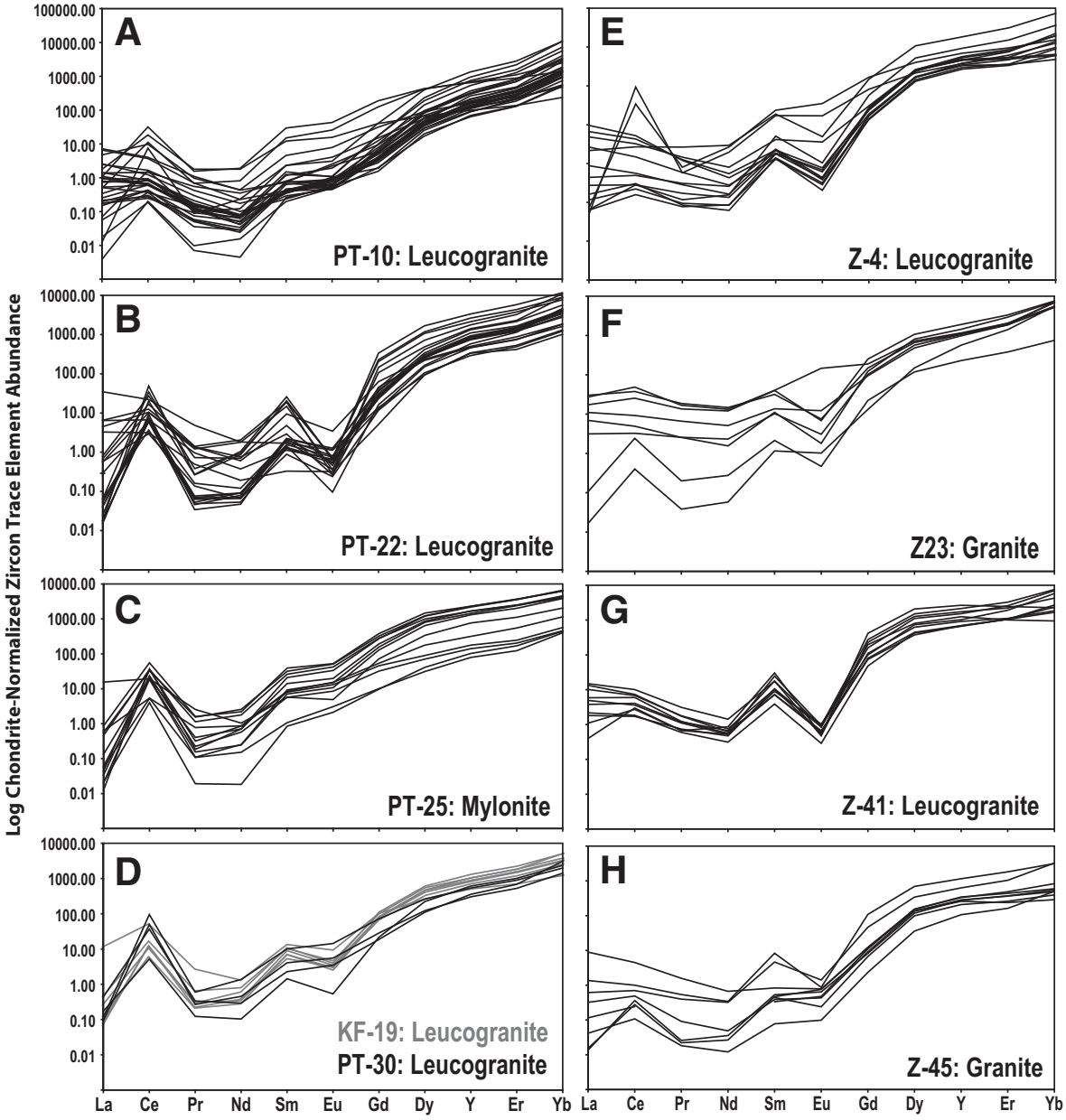

Figure 7. Rare earth element (REE) diagrams corresponding to U-Pb sensitive high-resolution ion microprobe (SHRIMP) analyses of zircon. Trace-element abundances are chondrite-normalized (McDonough and Sun, 1995) and given in ppm. Most samples show negative Eu anomalies that indicate coeval zircon and plagioclase growth.

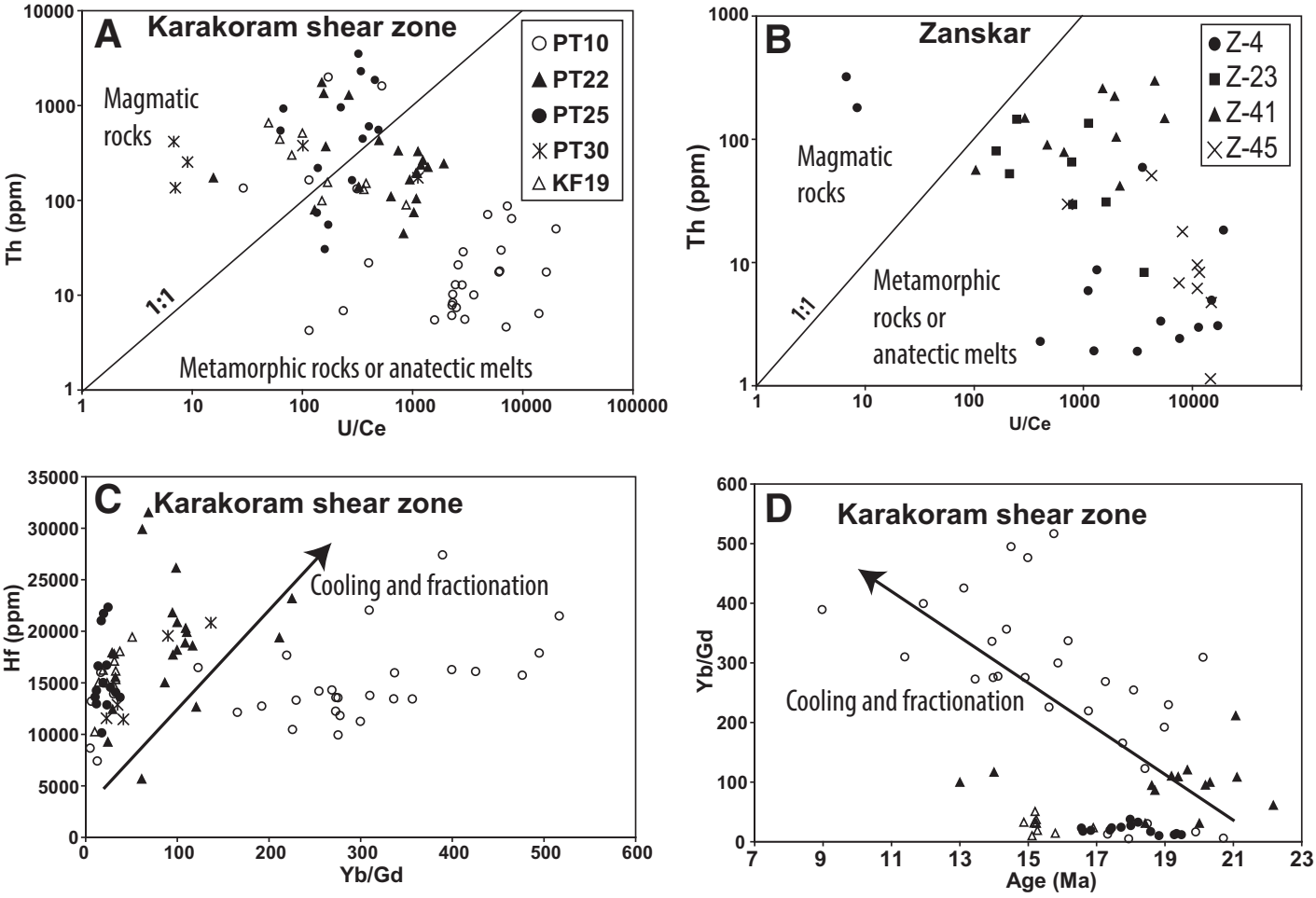

Figure 8. Sensitive high-resolution ion microprobe (SHRIMP) zircon geochemistry plots for Oligocene–Miocene leucogranites and PT-25 mylonite. (A) Th vs. U/Ce plot for Karakoram shear zone samples that characterizes zircon crystallization as both magmatic and metamorphic/anatectic. (B) Th vs. U/Ce plot for Zanskar samples showing nearly exclusive metamorphic/anatectic signatures. (C) Hf vs. Yb/Gd plot for Karakoram shear zone samples showing a positive relationship between Yb/Gd and Hf that demonstrates cooling and fractionation. (D) Yb/Gd ratio vs. ^{207}Pb-corrected $^{206}Pb/^{238}U$ age plot for Miocene Karakoram shear zone samples that shows enrichment of heavy rare earth elements over time, especially for leucogranite sample PT-10 (note that Jurassic PT-30 data points are not within the bounds of this plot).

Th classification suggests that PT-22 zircons crystallized both under magmatic and anatectic conditions (Fig. 8A). Although PT-22 cores and rims have greater Eu anomalies than PT-10, they show no enrichment of Hf or HREEs relative to age (Figs. 8C and 8D). Seventeen spot analyses of PT-22 Paleocene through Eocene zircon cores yielded $\varepsilon_{Hf}(t)$ values from +1.7 to +9.1 (Fig. 9A).

PT-25: Quartzofeldspathic Mylonite

This quartzofeldspathic mylonite from the Tangste strand of the Karakoram shear zone near Tangste Monastery (Figs. 2 and 4) has feldspar sigma clasts ~5 mm in diameter (Fig. 5C). Field relationships suggest that PT-25 is mylonitized leucogranite from the same body as sample PT-22. Fourteen SHRIMP spot analyses of oscillatory-zoned zircon rims range from 19.5 Ma to 16.6 Ma, and eight LA-ICP-MS Miocene spot ages for zircon cores range from 22.8 Ma to 17.8 Ma (Figs. 6E and 6F). Eight luminescent zircon cores provide a mean inherited age of 85.7 ± 1.4 Ma (Fig. 6F); three concordant ages were excluded from this mean because they likely resulted from mixing between core and rim ages. Both rims and euhedral cores have Miocene ages that exhibit nearly identical trace-element patterns, showing only slight Eu anomalies (Fig. 7C), and lower Yb/Gd ratios than for either PT-10 or PT-22 (Fig. 8C). Corresponding U/Ce ratios and Th content suggest primarily magmatic crystallization (Fig. 8A). The cluster of eight Cretaceous zircon cores have $\varepsilon_{Hf}(t)$ values from +3.5 to +7.5 (Fig. 9B); four spot ages have $\varepsilon_{Hf}(t)$ values from +1.1 to +2.7, and one Miocene age spot has an abnormally low $\varepsilon_{Hf}(t)$ value of –8.6.

PT-30: Nondeformed Leucogranite Dike

This fine-grained nondeformed leucogranite dike intrudes diorite north of the Pangong strand of the Karakoram shear zone on the northern side of the Shyok valley in the Karakoram Range (Figs. 2 and 4). Only one age (18.9 ± 0.3 Ma) was obtained from a thin, nonluminescent zircon rim, but oscillatory-zoned cores yielded a concordant cluster of combined SHRIMP and LA-ICP-MS ages averaging 157 ± 3 Ma (Fig. 6G) and a mixing line with an upper intercept of 802 ± 34 Ma. Jurassic domains have minor Eu anomalies and are enriched in HREEs (Fig. 7D). Yb/Gd ratios and Hf concentrations increase as Jurassic ages decrease (Fig. 8C), and U/Ce and Th concentrations (Fig. 8A) are consistent magmatic crystallization. Jurassic to Early Cretaceous zircons have $\varepsilon_{Hf}(t)$ values ranging from –8.8 through –1.1 (Fig. 9C). Ages on the mix-

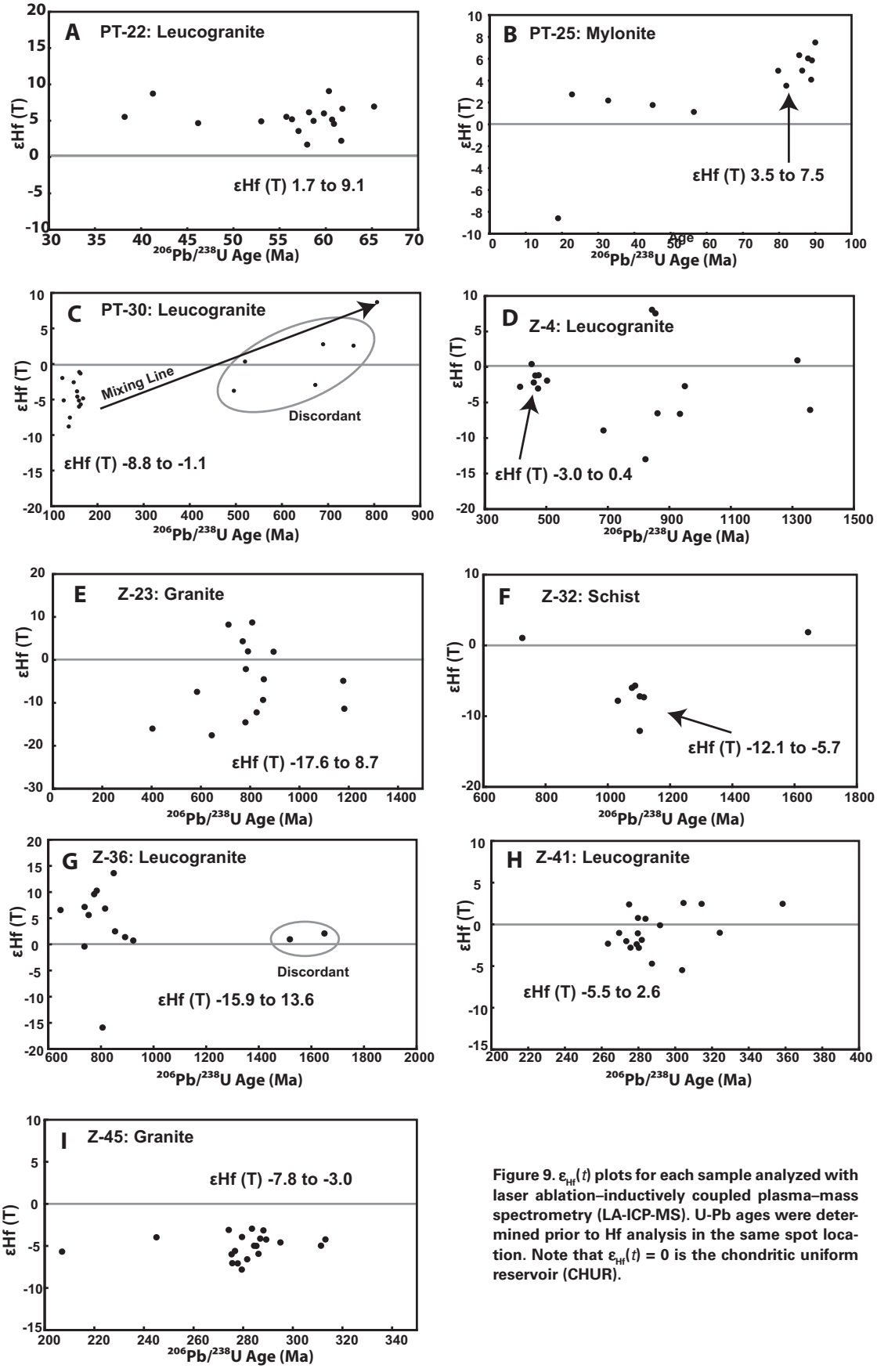

Figure 9. $\varepsilon_{Hf}(t)$ plots for each sample analyzed with laser ablation–inductively coupled plasma–mass spectrometry (LA-ICP-MS). U-Pb ages were determined prior to Hf analysis in the same spot location. Note that $\varepsilon_{Hf}(t) = 0$ is the chondritic uniform reservoir (CHUR).

Lithosphere, published online on 20 April 2013 as doi:10.1130/L213.1

ing line have a range of $\varepsilon_{Hf}(t)$ values from –3.7 through +8.7.

KF-19: Nondeformed Leucogranite Dike

KF-19 is from a nondeformed leucogranite dike intruded into the Nubra Formation from above the Samstanling Monastery near Sumur in the Nubra valley (Fig. 2). The Nubra Formation includes metavolcanics, greenschist-facies shale, and serpentinized pyroxenite. Euhedral oscillatory-zoned zircons range from 25.7 to 14.0 Ma, with a prominent cluster at ca. 15 Ma (Fig. 6H). Trace-element plots show moderate Eu anomalies (Fig. 7D) and low Yb/Gd ratios (Fig. 8D) that compare closely to PT-25 values.

Zanskar Region

Z-1: Migmatite

This migmatized and highly strained orthogneiss lies structurally beneath leucogranite lenses in the Haptal valley near Padum (Fig. 3), less than 5 km south of the Zanskar shear zone. Fibrous sillimanite lies within the foliation and wraps around abundant kyanite and garnet (Fig. 10C). Monazites provide an average $^{232}Th/^{208}Pb$ age of 21.5 ± 1.0 Ma (Table 1). In thin section, monazites are observed primarily within quartz grains.

Z-4: Foliated Leucogranite Pluton

This sample is from an ~1-km-wide deformed leucogranite pluton/lens in the Haptal valley, below metapelitic schists and above migmatized orthogneiss to the south (Figs. 3 and 11A). Euhedral and oscillatory-zoned zircons have 15 concordant U-Pb ages from 475 to 410 Ma (Fig. 6J). Ten monazite $^{232}Th/^{208}Pb$ ages have an average age of 461 ± 21 Ma (Table 1); electron microprobe images of Z-4 monazites exhibit sector zoning for Y and Th/U concentrations (Fig. 12). Several inherited zircon core ages appear to lie on two separate mixing lines, with Paleozoic lower intercepts and Precambrian upper intersects at 918 ± 68 Ma and 1548 ± 82 Ma, respectively (Fig. 6I). Two SHRIMP analyses of oscillatory-zoned rims provide ages of 27.2 ± 0.2 and 21.6 ± 0.1 Ma. Most Z-4 Paleozoic zircons have negative Eu anomalies and HREE enrichment (Fig. 7E). Paleozoic spots have $\varepsilon_{Hf}(t)$ values from –3.0 to +0.4, and Precambrian spots range from –13.0 to +8.0 (Fig. 9D).

Z-5: Nondeformed Leucogranite Dike

Z-5 is from a nondeformed leucogranite pegmatite dike that crosscuts the deformed Haptal valley leucogranite pluton/lens. Z-5 monazites have an average $^{232}Th/^{208}Pb$ age of 20.3 ± 1.7 Ma (Table 1). Three spot analyses yielded older ages, probably from mixing with inherited Paleozoic monazite domains, as seen in Z-4.

Z-23: Granite

This coarse-grained granite crops out at Pensi La at the head of the Zanskar/Doda River (Fig. 3). Zircons have multiple age domains: Nonluminescent rims have ages from 230 to 180 Ma, and cores have scattered Proterozoic ages and a cluster of ages between 895 and 712 Ma (Figs. 6K and 6L). Zircons have negative Eu anomalies (Fig. 7F), but Ce anomalies are less pronounced, and the U/Ce versus Th plot classifies them as metamorphic or anatectic (Fig. 8B). Z-23 LREE enrichment increases as ages decrease, as shown by the Th/Ce ratios. Z-23 monazites have an average $^{232}Th/^{208}Pb$ age of 436 ± 25 Ma (Table 1), which coincides with the several Paleozoic zircon ages from this sample and monazite and zircon ages in sample Z-4. The $\varepsilon_{Hf}(t)$ values associated with 2500–400 Ma spots range widely, from –17.6 to +8.7, with one anomalously low analysis of –48; there is no apparent relationship between age and Hf isotopic ratios (Fig. 9E).

Z-32 and Z-40: Garnet Schists

These highly deformed garnet schists are from the upper Greater Himalayan Sequence

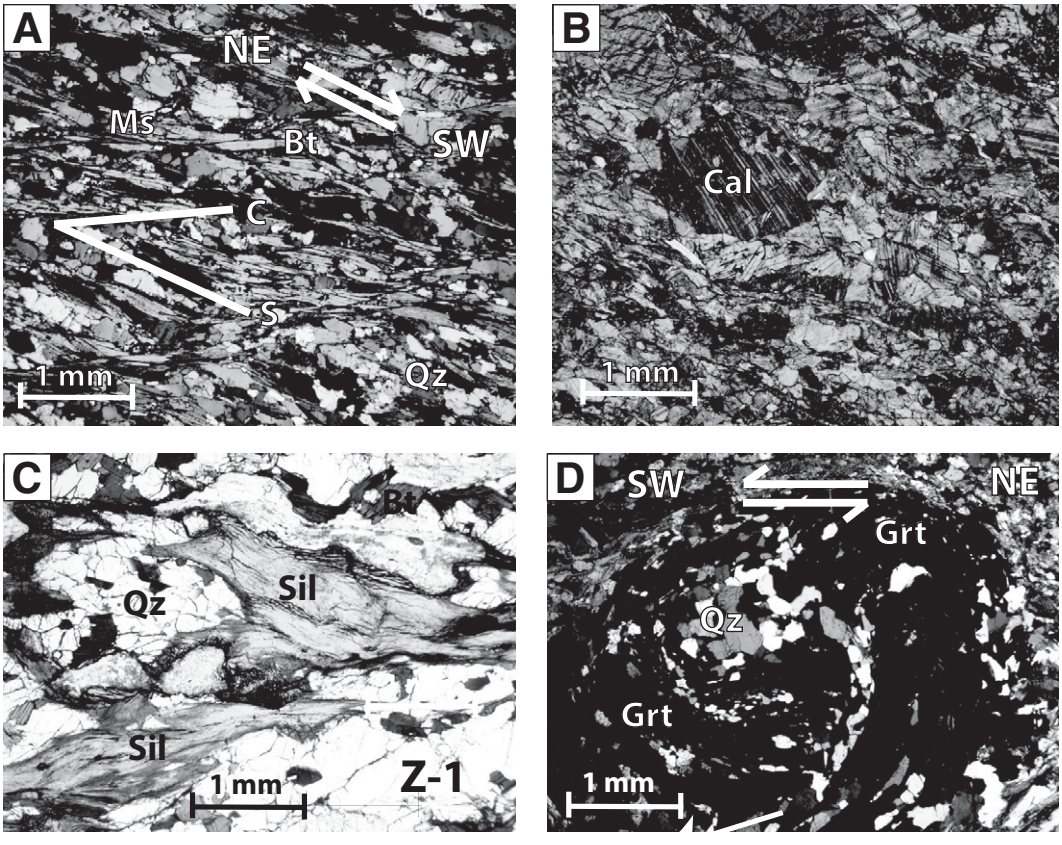

Figure 10. Photomicrographs of thin sections from Zanskar samples. (A) Mica schist in the upper Greater Himalayan Sequence northeast of sample Z-4 with S-C fabric that preserves an earlier top-to-the-SW shear sense. (B) A calc-silicate augen in mylonite near Rangdum, immediately east of sample Z-32 (cross polarized light). (C) Orthogneissic migmatite (Z-1) with fibrous sillimanite where leucocratic melt escaped (plane polarized light). (D) Snowball garnet in Greater Himalayan Sequence schist (Z-40) showing prograde synkinematic growth during top-to-the-SW shear sense. The Data Repository contains a color version of this figure (see text footnote 1). Mineral abbreviations after Whitney and Evans, 2010.

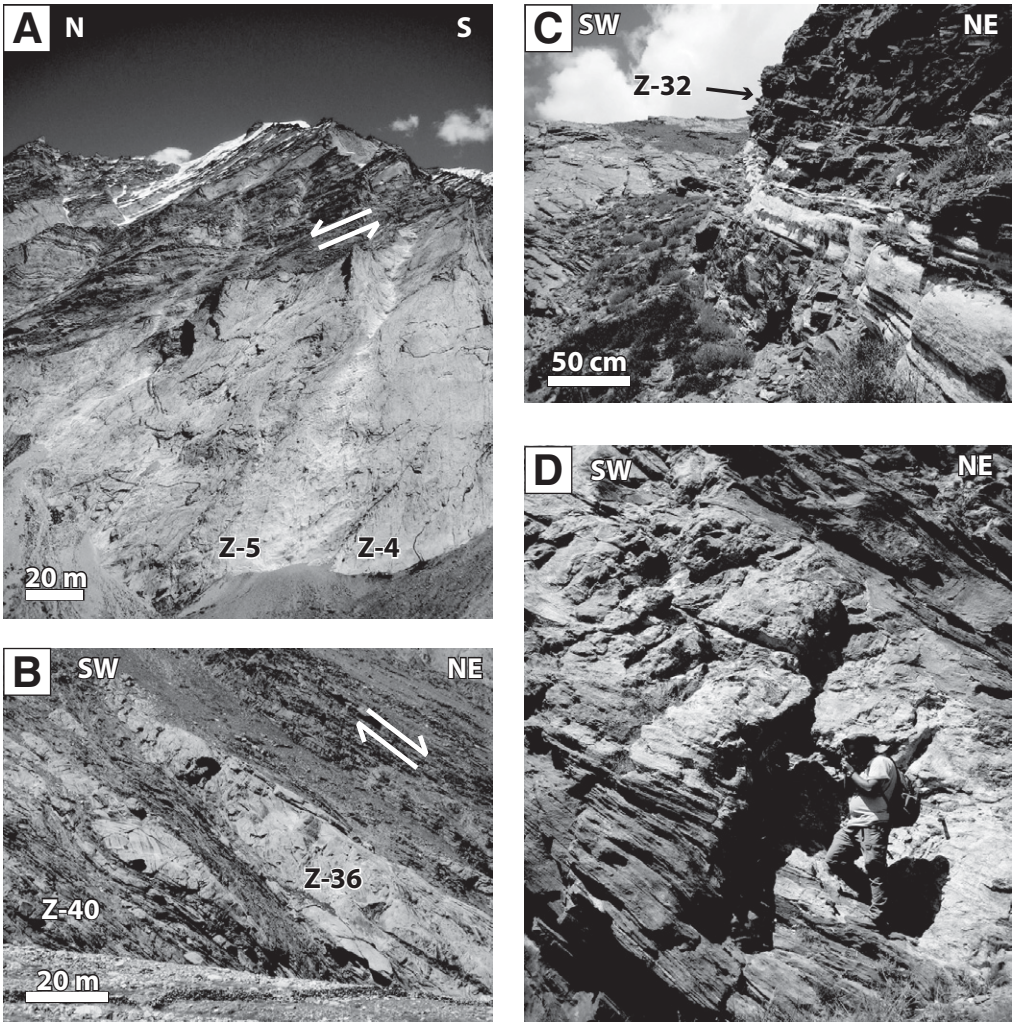

Figure 11. Field photographs from the Zanskar field area. (A) Small leucogranite bodies and migmatite above the Haptal valley pluton across from samples Z-4 and Z-5. (B) Foliated granite intrusions (Z-36) showing pre- to syn-kinematic emplacement into the surrounding Greater Himalayan Sequence schist (sample Z-40) in Nun-Kun valley. (C) Leucogranite sill in schist in the easternmost part of the Nun-Kun valley (sample Z-32). (D) Granite sill deformed and folded along with surrounding Greater Himalayan Sequence gneiss (34°05′14.7″N, 76°00′32.0″E). The Data Repository contains a color version of this figure (see text footnote 1).

in the Nun-Kun valley (Figs. 3, 11B, and 11C) southwest of mylonitized calc-silicate (Fig. 10B). Mica schists contain hornblende and garnet porphyroblasts, and have ~1-cm-thick boudinaged quartz veins. An S-C fabric (Fig. 10A) and snowball garnet porphyroblasts (Fig. 10D) in these schists show top-to-the-SW shear sense. LA-ICP-MS analyses for Z-32 give six zircon ages from 1100 to 995 Ma, with $\varepsilon_{Hf}(t)$ values from –12.1 to –5.7, and two outliers at ca. 1650 Ma and ca. 725 Ma (Figs. 6M and 9F). Z-40 has monazites with Y-enriched and slightly Th/U-depleted rims (Fig. 12); SHRIMP analyses yield a mean $^{232}Th/^{208}Pb$ age of 27.3 ± 1.2 Ma (Table 1).

Z-36: Foliated Leucogranite Lens

Z-36 is from a foliated and boudinaged leucogranite lens in metapelitic schists northeast of larger leucogranite bodies in the Nun-Kun valley (Figs. 3 and 11B). Zircon rims were too thin to target for dating, but 11 concordant zircon ages from Precambrian cores average 804 ± 27 Ma (Fig. 6N); $\varepsilon_{Hf}(t)$ values range from –15.9 to +13.6 (Fig. 9G). Five analyses were discarded due to mixing of younger and older age domains.

Z-41: Deformed Leucogranite Pluton

This sample is from a deformed granite pluton in the Nun-Kun valley (Fig. 3) with strained orthoclase grains >1 cm in diameter. Twenty-nine concordant ages from SHRIMP and LA-ICP-MS analyses of euhedral, oscillatory-zoned zircons produced ages from 360 Ma to 264 Ma (Fig. 6O). These Mississippian–Permian analyses have no Ce anomalies, pronounced Eu anomalies (Fig. 7G), metamorphic or anatectic U/Ce and Th values (Fig. 8B), and $\varepsilon_{Hf}(t)$ values from –5.5 to +2.6 (Fig. 9H).

Z-45: Deformed Granite

This deformed granite was sampled from the lowest structural level observed in the northwestern Greater Himalayan Sequence near Suru village (Fig. 3) and has been folded with adjacent metasedimentary rocks and migmatites (Fig. 11D). Nonluminescent oscillatory-zoned rims on euhedral zircons provide concordant ages of 47–25 Ma (Fig. 6P), and zircon cores are Early Permian, averaging 284 ± 4.4 Ma (Fig. 6Q). Because thin zircon rims were difficult to isolate, ages between 250 Ma and 35 Ma are likely caused by mixing between the Cenozoic rims and Permian cores. Permian zircon spot analyses have no Ce anomalies, pronounced Eu anomalies (Fig. 7H), and metamorphic or anatectic U/Ce and Th values (Fig. 8B). Permian zircon analyses have $\varepsilon_{Hf}(t)$ values from –7.8 to +3.0 (Fig. 9I). Anhedral and irregularly zoned monazites (Fig. 12) have an average $^{232}Th/^{208}Pb$ age of 17.2 ± 0.9 Ma (Table 1).

DISCUSSION

Timing of Karakoram Shear Zone Magmatism

Our results largely corroborate previous geochronology reported in Tangste gorge, but they record a more protracted magmatic history that

Lithosphere, published online on 20 April 2013 as doi:10.1130/L213.1

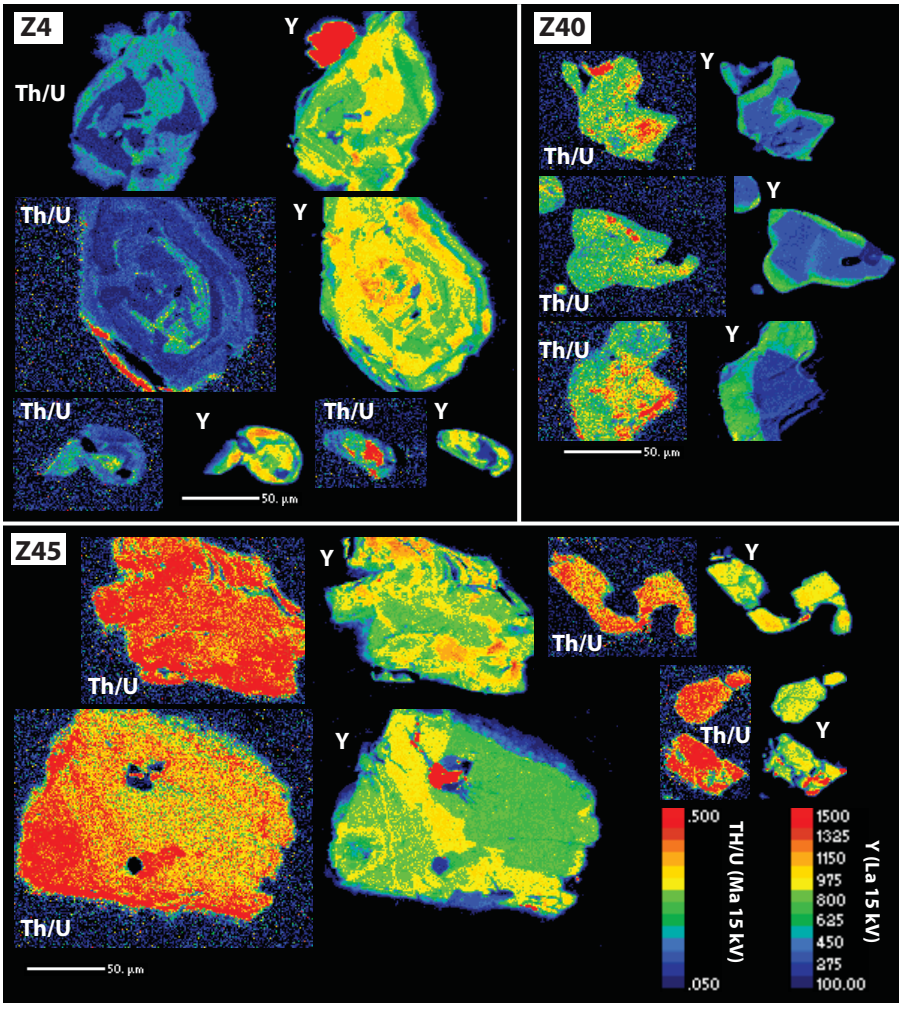

Figure 12. Electron probe micro-analyzer scans of Zanskar monazites showing compositional zoning of Y and the Th/U ratio. Euhedral Z-4 monazites exhibit sector zoning indicative of an igneous origin (Parrish, 1990). In contrast, metamorphic Z-40 monazites are anhedral and display two distinct growth zones suggestive of episodic metamorphic growth (Zhu and O'Nions, 1999); the outer zone with higher Y concentrations may indicate that outer monazite growth postdates garnet growth because Y is preferentially incorporated into garnet (Pyle and Spear, 2003). Z-45 monazites have irregular Y zoning, from intergrowth crystallization (Zhu and O'Nions, 1999), overgrowth on monazites with complex geometries (Spear and Pyle, 2002), or fluid-related alteration and resetting (Williams et al., 2011). Anhedral Z-45 monazites contrast with euhedral igneous Z-4 monazites, suggesting that Z-45 monazites are metamorphic. The absence of garnet in the Z-45 igneous protolith can explain the absence of Y-rich rims observed for Z-40 under similar metamorphic conditions.

lasted >10 m.y. The Pangong strand of the Karakoram shear zone in Tangste gorge contains the migmatized granitic Muglib pluton (Fig. 5A; also referred to as Muglib batholith), which has chemical and isotopic similarities to the Ladakh batholith (Weinberg and Dunlap, 2000; Ravikant et al., 2009; Reichardt et al., 2010) and previously determined U-Pb zircon ages of 106 ± 2.3 Ma, 72.8 ± 0.9 Ma, 71.4 ± 0.6 Ma, and 22–15 Ma (Searle et al., 1998; Reichardt et al., 2010). Most PT-10 ages are ca. 18–17 Ma, corresponding closely to nearby leucogranite ages of 18.0 ± 0.4 Ma (Reichardt et al., 2010) and 17.3 ± 0.1 Ma (Phillips et al., 2004). Reichardt et al. (2010) noted a zircon crystallization age range of 18.0–15.1 Ma, which is also documented in the adjacent migmatized pelites and the Muglib pluton (Searle et al., 1998; Phillips and Searle, 2007). Our trace-element data for PT-10 show that the emplacement of the Tangste pluton occurred over an extended period of fractionation during cooling, as seen in Yb/Gd versus Hf trends, lasting >10 m.y. from ca. 21 Ma to 9 Ma (Figs. 8C and 8D). Although this age range could be explained by mixing of subpopulations or continuous crystallization, the preponderance of ca. 18 Ma ages may indicate a pulse of magmatism and crystallization at that time, followed by continuous or pulsed crystallization.

Zircon rim ages for PT-22 leucogranite (22.2–18.4 Ma) and PT-25 mylonite (19.3–16.6 Ma) correspond to previously reported ages of 22–13 Ma in Tangste gorge (Boutonnet et al., 2012, and references therein), and they represent continuous or episodic crystallization. The inherited zircon ages of 65–38 Ma presented here compare to inherited zircon ages for the Karakoram shear zone of 69–56 Ma (Jain and Singh, 2008; Ravikant et al., 2009). Tangste mylonite sample PT-25 contains several concordant inherited core ages averaging 85.7 ± 1.4 Ma (Fig. 6F), i.e., slightly older than the 75.5 ± 1.0 Ma age obtained from the same mylonite by Jain and Singh (2008). To the northwest in Nubra valley, a leucogranite KF-19 has concordant ages ranging from 40 Ma to 14 Ma (Fig. 6H) and a cluster of ages at 15 Ma comparable to the 15.0 ± 0.4 Ma Satti leucogranite (Weinberg and Dunlap, 2000).

Combined with previous literature, this study demonstrates that the onset of leucogranite crystallization occurred at 22–21 Ma throughout Tangste gorge. The predominance of 19–18 Ma ages observed in Tangste gorge may reflect a period of magma accumulation and injection during dilational transcurrent fault motion (Weinberg et al., 2009). Our results are consistent with the proposal by Rutter et al. (2007) that shearing along the northern Pangong strand of the Karakoram shear zone may have outlived motion along the Tangste strand, because the youngest granites were exhumed near the Pangong strand.

Origins of the Karakoram Shear Zone Granites

Different sources have been proposed for the Karakoram shear zone leucogranites: the proximal Karakoram terrane and Ladakh batholith (Weinberg et al., 2009; Reichardt et al., 2010), subducted Indian crust (Leech, 2008), or a combination of the two (Ravikant et al., 2009). Geochronologic constraints and isotopic data for these various lithotectonic units are presented next in order to interpret the source of Karakoram shear zone leucogranites.

Indian Himalaya

Detrital zircon analyses of Indian Himalayan units from the Greater Himalayan Sequence in Sutlej valley give ages from Paleoproterozoic through Cambrian and $\varepsilon_{Hf}(t)$ values from –25 to +5 (Richards et al., 2005), and the Archean Aravalli craton in northwest India has values that range from –27 to +8 (Condie et al., 2005), which correspond well with Zanskar $\varepsilon_{Hf}(t)$ values from –18 to +14 (Fig. 13). The samples

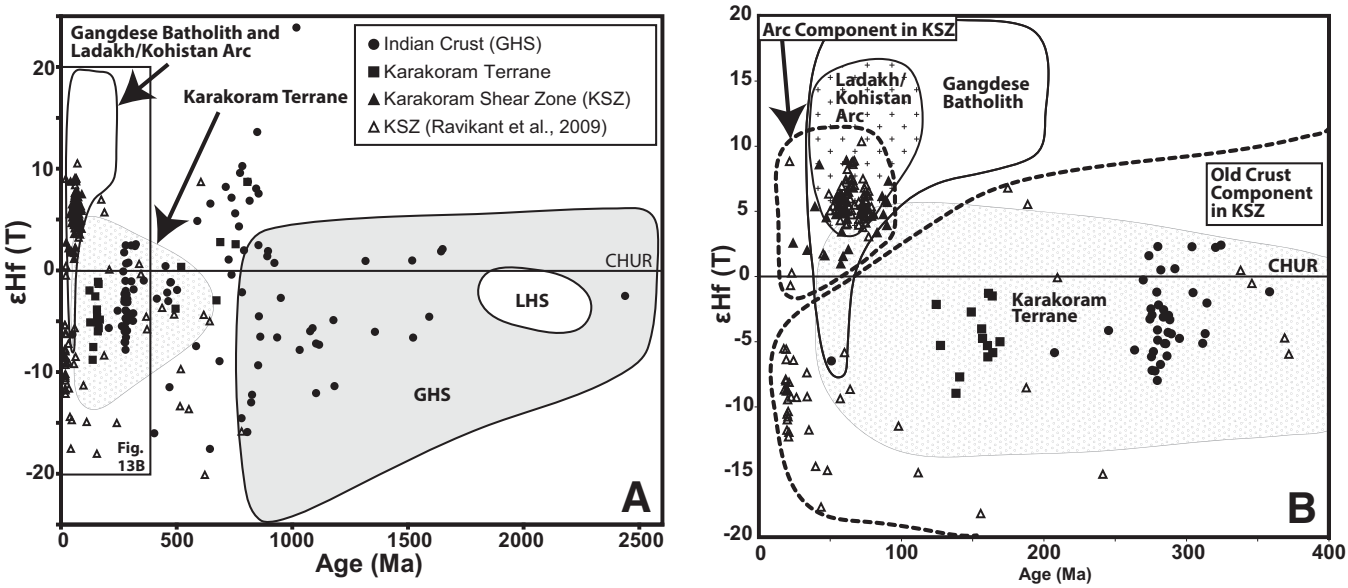

Figure 13. (A) Initial ε_{Hf} values ($^{177}Hf/^{176}Hf$ ratios at the time of crystallization normalized to chondritic uniform reservoir [CHUR]), plotted against U-Pb age for Karakoram shear zone and Zanskar. Karakoram shear zone data points from Ravikant et al. (2009) are included. Shaded regions are shown for the Gangdese batholith (Chu et al., 2006; Wu et al., 2007; Chiu et al., 2009), the Ladakh/Kohistan arc region (Schaltegger et al., 2002; Heuberger et al., 2007; Ravikant et al., 2009; Bouilhol et al., 2010a), and Karakoram terrane (Heuberger et al., 2007; Ravikant et al., 2009; Bouilhol et al., 2010a). Karakoram shear zone leucogranites have a range of $\varepsilon_{Hf}(t)$ values that suggest mixing between two sources: the Ladakh/Kohistan arc and an older crustal component (either the Karakoram terrane or Indian crust). The black rectangle on the left is the area plotted in B. (B) ε_{Hf} vs. U-Pb age diagram for Karakoram shear zone and Zanskar. Shaded regions are shown for the Gangdese batholith and Ladakh/Kohistan arc (Schaltegger et al., 2002; Chu et al., 2006; Heuberger et al., 2007; Wu et al., 2007; Chiu et al., 2009; Ravikant et al., 2009; Bouilhol et al., 2010a), the Karakoram terrane (Heuberger et al., 2007; Ravikant et al., 2009), and Indian crust (Greater Himalayan Sequence [GHS] and Lesser Himalaya Sequence [LHS]; Richards et al., 2005). A single Greater Himalayan Sequence data point falls outside this plot: $\varepsilon_{Hf}(t)$ is –48 at 3325 Ma.

analyzed for this study were primarily granitic, which may account for higher $\varepsilon_{Hf}(t)$ values and younger ages than obtained in earlier detrital zircon studies (see Data Repository [see footnote 1]). The Lesser Himalaya Sequence in Sutlej valley has $\varepsilon_{Hf}(t)$ values that range from –5.7 to –0.9 (Richards et al., 2005), while Mississippian–Permian granites in the Zanskar Greater Himalayan Sequence range from –8 to +2.5 (Fig. 13). Overall, the Greater Himalayan Sequence radiogenic Hf signature records prolonged crustal evolution and is largely indistinguishable from other terranes accreted to Asia.

Ladakh-Kohistan-Gangdese Batholiths

Neotethyan oceanic subduction–related batholiths across the Himalayan orogen have comparable mantle-enriched Hf signatures (Fig. 13). In the west, 112–85 Ma Kohistan granites have $\varepsilon_{Hf}(t)$ values from +10 to +16 (Schaltegger et al., 2002; Heuberger et al., 2007; Bouilhol et al., 2010a), and Paleogene granites have values from +5 to +12 (Heuberger et al., 2007). The Ladakh batholith granites have ages spanning 103–50 Ma, with most ages ranging from 68 Ma to 50 Ma (Honegger et al., 1982; Weinberg and Dunlap, 2000; Jain and Singh, 2008). Ravikant et al. (2009) reported Paleogene ages for the Ladakh batholith with $\varepsilon_{Hf}(t)$ values from +6.4 to +10.3 and T_{DM} ages of ca. 700–500 Ma (Bouilhol et al., 2010b). The Chogdo Formation of the Indus molasse has zircon ages of ca. 100–50 Ma and $\varepsilon_{Hf}(t)$ values from +4 to +15 related to deposition of Ladakh batholith sediments prior to collision with India (Wu et al., 2007). To the east, the Gangdese batholith contains three zircon populations: 205–152 Ma with $\varepsilon_{Hf}(t)$ values of +10 to +18, 109–80 Ma with $\varepsilon_{Hf}(t)$ values of about +5 to +20, and 65–41 Ma with $\varepsilon_{Hf}(t)$ values of about –5 to +15 (Chu et al., 2006; Chiu et al., 2009; Ji et al., 2009).

Lhasa and Karakoram Terranes

Early Cretaceous and Paleocene magmatism in the Lhasa block occurred at the same time as Gangdese magmatism to the south, but with lower $\varepsilon_{Hf}(t)$ values from –20 to +5 and T_{DM} ages from 0.8 to 2.4 Ga (Figs. 13 and 14; Chu et al., 2006; Chiu et al., 2009). Detrital zircon records from the Lhasa block have dominant age populations of 1400–1000 Ma, 600–500 Ma, and 100–150 Ma (Leier et al., 2007). Based on these studies, Lhasa block U-Pb and Hf signatures are largely distinct from those of the Gangdese batholith.

In Pakistan, Karakoram granites and diorites have inherited ages of 1620–725 Ma and a mean crystallization age of 104 Ma and $\varepsilon_{Hf}(t)$ values from –5 to +5 (Fig. 13; Heuberger et al., 2007). Along the Karakoram shear zone, tonalite enclaves attributed to the Karakoram terrane have a similar age of 103 Ma and $\varepsilon_{Hf}(t)$ values of –4 to –2 (Ravikant et al., 2009). North of the Shyok suture, the Tirit granite has a Cretaceous–Paleocene signature similar to the Ladakh batholith (Weinberg and Dunlap, 2000). Northwest of the Karakoram shear zone, the Karakoram batholith has whole-rock Rb-Sr ages of 118 ± 15 Ma and 115 ± 18 Ma (Ravikant, 2006) and was intruded by Miocene leucogranites ca. 25 Ma and younger (Schärer et al., 1990; Ravikant et al., 2009). Results from the Shyok valley in this study reveal a previously undocumented zircon population with a mean age of 157 Ma and $\varepsilon_{Hf}(t)$ values from –8.8 to –1.1 (Fig. 6G), similar to Baltoro granites SW of the Karakoram shear zone, which have $\varepsilon_{Hf}(t)$ values from –8.0 to –1.8 and are presumed to have been derived from partial melting of mafic Karakoram lower crust at 26–21 Ma (Mahéo et al., 2009), whereas T_{DM} ages for the Shyok valley sample are 1.3–0.8 Ga, comparable to results from the Lhasa block (Figs. 13 and 14; Chu et al., 2006; Wu et al., 2007). However, both the Karakoram and Lhasa terranes have old crustal signatures that may be largely indistinguishable. Late Miocene syenite and lamprophyre intrusions in the Karakoram

Lithosphere, published online on 20 April 2013 as doi:10.1130/L213.1

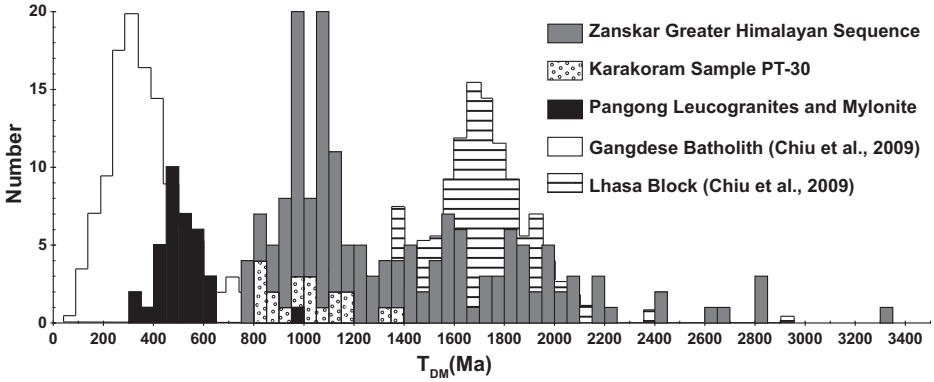

Figure 14. Histogram for zircon T_{DM} (zircon Hf isotope crustal model age) for Zanskar and Karakoram fault samples in comparison to the eastern Himalaya Gangdese batholith and Lhasa block published by Chiu et al. (2009). Data from Chiu et al. (2009) have been scaled along the *y*-axis to fit our data.

terrane south of the Karakoram shear zone have depleted mantle signatures and $\varepsilon_{Hf}(t)$ values of +10.4 to +11.2 (Mahéo et al., 2002, 2009).

Karakoram Shear Zone Leucogranites

Leucogranites from the Karakoram shear zone in Tangste gorge have Cretaceous–Paleocene zircon cores, and most $\varepsilon_{Hf}(t)$ values range from +1 to +9, which compare most closely to Ladakh-Kohistan-Gangdese arc units but overlap with Karakoram batholith analyses presented by Heuberger et al. (2007) (Fig. 13). T_{DM} model ages for Tangste gorge leucogranites also overlap with Gangdese arc values, except for one analysis, which coincides with both Karakoram terrane and the Greater Himalayan Sequence (Fig. 14; Chiu et al., 2009). T_{DM} model ages are a means of isotopically classifying lithotectonic units, but model ages can be skewed by crustal fractionation and are based on assumptions about the isotopic composition of the mantle source material (Gehrels, 2010); because of these uncertainties, the T_{DM} model ages presented here are not considered accurate indicators of the time at which crustal magmas were separated from the upper mantle.

The dominantly positive $\varepsilon_{Hf}(t)$ signature for Karakoram shear zone leucogranites suggests that arc-related units were the primary sources of magmas in Tangste gorge (Fig. 13). Near Darbuk, 15 km to the northwest, granites have older crustal inheritance and $\varepsilon_{Hf}(t)$ values from –10.5 to –8.5 (Jain and Singh, 2008; Ravikant et al., 2009); Ravikant et al. (2009) interpreted the low $\varepsilon_{Hf}(t)$ values for the Darbuk granites as having input from the Indian crust. Those $\varepsilon_{Hf}(t)$ values contrast with data from Tangste gorge values (with the exception of a single –8.6 value for PT-25 spot 5C; Fig. 13A), indicating that magma sources differ along strike in the Karakoram shear zone. Anomalously low $\varepsilon_{Hf}(t)$ values in the Darbuk granites can be explained by input of magmas from the adjacent Karakoram terrane or underlying Indian crustal units, but insufficient data exist to distinguish between the Karakoram terrane and subducted Indian crust (both have low $\varepsilon_{Hf}[t]$ values associated with Gondwanan zircon inheritance; Fig. 13). It is unclear whether the Karakoram terrane underwent Cretaceous–Paleocene magmatism similar to the Ladakh batholith (see Schärer et al., 1990; Weinberg and Dunlap, 2000), and these results neither strongly support nor refute the hypothesis that the Karakoram shear zone acted as a conduit for the ascent of partially molten Indian crust (see discussions in Leech, 2008; Leloup et al., 2011).

Zanskar Geochronology

Cambrian–Ordovician monazite and zircon ages for granite bodies in the Haptal valley and at Pensi La correspond to Greater Himalayan Sequence ages previously determined using whole-rock Rb-Sr data (Frank et al., 1977; Mehta, 1977; Stutz and Thöni, 1987), U-Pb monazite ages (Noble and Searle, 1995; Walker et al., 1999), and U-Pb zircon geochronology (Pognante et al., 1990; Noble and Searle, 1995) (Fig. 15). Mississippian–Permian zircon ages have been documented both in Zanskar (Noble et al., 2001) and elsewhere in the northwest Himalaya (Honegger et al., 1982; Spring et al., 1993; Inger, 1998). Noble et al. (2001) noted that Permian granite sills have been folded and deformed along with surrounding metasediments at the deepest structural units of the Suru dome (Fig. 3). This study shows that Mississippian–Permian granites also exist among the kilometer-scale folds in northwest Zanskar (e.g., Z-41), but detailed field mapping and additional geochronology across the region would be necessary to determine the size and extent of these pre-Himalayan granite intrusions.

Miocene igneous monazite ages have been reported at Gumberanjun (22.2 ± 0.2 Ma—Dézes et al., 1999; 22.1 ± 0.4 Ma—Walker et al., 1999), Umasi La (20.5–19.6 Ma; Noble and Searle, 1995), and Shafat (20.8 ± 0.3 Ma; Noble and Searle, 1995). The same units at Gumberanjun have $^{40}Ar/^{39}Ar$ muscovite ages only slightly younger than the monazite ages from leucogranite (ca. 21–20 Ma rather than ca. 22–21 Ma),

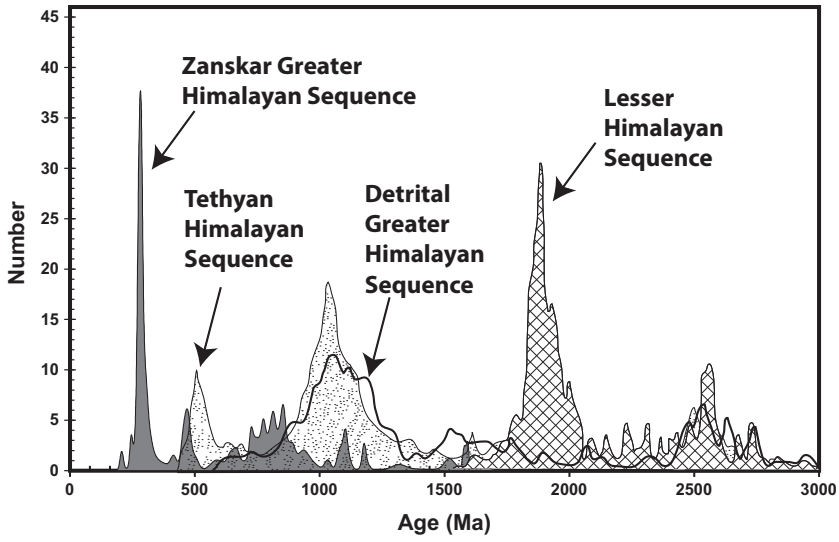

Figure 15. Probability density plot showing laser ablation–inductively coupled plasma–mass spectrometry (LA-ICP-MS) zircon ages for Zanskar (gray) in comparison to detrital zircon ages acquired by DeCelles et al. (2000); the scale only represents Zanskar data from this study.

but they are significantly younger than nearby metapelites, which have metamorphic monazite ages of 32–29 Ma (Walker et al., 1999). Peak prograde metamorphism between 33 and 27 Ma occurred at 620–650 °C and >0.95 GPa in southeast Zanskar (Vance and Harris, 1999; Walker et al., 2001) and ~700 °C and 1.0 GPa in northwest Zanskar (Vance and Harris, 1999), conditions sufficient for metamorphic monazite growth (e.g., Pyle and Spear, 2003; Rubatto et al., 2001). Monazite dating of a mica schist from this study records peak metamorphism at ca. 27.3 ± 1.2 Ma for the Suru valley (Z-40; Table 1). High-temperature retrograde metamorphic conditions likely persisted through ca. 22 Ma (Walker et al., 1999) and may have persisted to 17.2 ± 0.9 Ma (Z-41; Table 1), based on a Th-Pb age for metamorphic monazite from this study (Fig. 12).

Zircon and monazite results for Haptal Tokpo and Suru dome record Cenozoic anatexis and metamorphic overprinting of pre-Himalayan granites, but the relative abundance of pre-Himalayan and Cenozoic granite remains unknown. This study reports Cenozoic ages for several euhedral zircon rims from Haptal Tokpo (27 Ma and 22 Ma, Z-4) and from near Suru dome (>26 Ma, Z-45). The Suru granite is Permian in age and folded within surrounding metasediments (Noble et al., 2001). Haptal Tokpo and Suru granite monazite ages are Paleozoic (samples Z-4 and Z-23) and Cenozoic (samples Z-1, Z-5, and Z-45). Paleozoic monazites are fairly euhedral and have concentric compositional zoning (Fig. 12) indicative of igneous growth conditions (e.g., Parrish, 1990), whereas Cenozoic monazites are anhedral and have irregular growth zones—likely caused by intergrowth crystallization (e.g., Zhu and O'Nions, 1999), complex internal geometries (e.g., Pyle and Spear, 2003), or fluid-related alteration (e.g., Williams et al., 2011)—characteristic of metamorphic growth conditions; differences in Th, U, and Y concentrations between samples are probably due to bulk rock composition differences rather than growth conditions. Based on these observations, we conclude that Cenozoic monazite growth occurred prior to (Z-40), during (Z-1), and after (Z-45) partial melting of the Greater Himalayan Sequence in Zanskar.

Exhumation of the Greater Himalaya Sequence in the Northwest Himalaya

The extent of Miocene anatectic melting in the northwestern Greater Himalayan Sequence contributes to our understanding of midcrustal exhumation mechanisms in the northwest Himalaya (Robyr et al., 2006). Geophysical data for the northwest Himalaya indicate <~5% partial melt in the midcrust, i.e., lower than required for ductile flow (Rosenberg and Handy, 2005; Unsworth et al., 2005; Arora et al., 2007; Caldwell et al., 2009). In Zanskar, the majority of migmatites are documented in Zanskar at Gumberanjun (Dézes et al., 1999; Walker et al., 1999; Robyr et al., 2002), Haptal Tokpo (Pognante, 1992), and the Bhazun gneiss dome (Kundig, 1989). The volume of Cenozoic melt in Zanskar remains controversial: The kilometer-scale granite bodies, melt-pods, dikes, and sills in northwest Zanskar have been described as either pre-Cenozoic crystalline basement deformed during the Himalayan orogeny (Honegger et al., 1982; Honegger, 1983; Herren, 1987b, 1988; Pognante, 1992) or as Miocene anatectic melts (Searle and Fryer, 1986; Rex et al., 1988; Searle and Rex, 1989; Gapais et al., 1992; Searle et al., 1992; Noble and Searle, 1995).

Zanskar granites appear to have the same cooling history as gneissic country rock (Gapais et al., 1992), and both igneous and metasedimentary samples yield Cenozoic monazite ages. Suru (Z-45) and Nun-Kun valley (Z-41) granites have been folded along with adjacent metasedimentary rock, and all Zanskar samples are foliated, except the Haptal Tokpo pegmatite (Z-5) and Pensi La granite (Z-23). These observations are consistent with abundant Paleozoic granites in Zanskar that underwent Cenozoic amphibolite- to granulite-facies metamorphism along with surrounding metasediments.

Although midcrustal exhumation occurred contemporaneously across the Himalaya (Noble and Searle, 1995), the Greater Himalayan Sequence in the northwest Himalaya appears to have undergone limited partial melting. Diversion of large volumes of midcrustal melts by the Karakoram shear zone seems improbable because the Karakoram shear zone does not contain abundant granites with Indian crustal affinity. Alternatively, low degrees of Cenozoic partial melting could be explained by the presence of mica-poor Paleozoic granites that lack the hydrous phases capable of producing large volumes of anatectic melt (Dézes et al., 1999). However, melting and exhumation are enhanced—rather than diminished—around domes with Paleozoic granite cores (Kundig, 1989). As predicted by numerical channel flow models (Beaumont et al., 2001) and proposed by Robyr et al. (2002) for the Gianbul dome, the weak low-grade metamorphic upper crust and a lack of efficient erosion in the northwest Himalaya could have led to the observed doming, which occurred well north of the range front, rather than exhumation of a partially melted middle crust in a typical channel flow model. In the western Himalaya, the crustal-scale Karakoram fault marks the modern northern limit of the subducting Indian crust, in stark contrast to the central and eastern Himalaya, where Indian crust underthrusts Tibet ~200 km north of the Indus-Yarlung suture zone (see Fig. 4 *in* Klemperer et al., 2013), and this could help explain the different exhumation style seen in the Greater Himalayan Sequence in Zanskar.

Synkinematic magmatism within the Karakoram shear zone began >22 Ma in the Pangong range (our data; Leloup et al., 2011; Boutonnet et al., 2012), and right-lateral deformation began prior to ca. 22.7 Ma along Ayilari segment of the fault (Valli et al., 2008). Similar estimates for the activation of the Zanskar shear zone prior to 22 Ma (Dézes et al., 1999) or at ca. 26 Ma (Robyr et al., 2006) suggest simultaneous movement along the Karakoram shear zone and South Tibetan detachment system beginning >22 Ma. South Tibetan detachment system shearing may have terminated earlier west of Gurla Mandata (at ca. 17 Ma) due to faulting associated with the Karakoram shear zone (Leloup et al., 2010). Our results and published geochronology are consistent with coeval movement along the South Tibetan detachment system and Karakoram shear zone between ca. 22 Ma and 17 Ma, when channel flow was active in the eastern Himalaya; simultaneous activity on these two major structures would certainly impact neo-Himalayan orogenic development in the western Himalaya.

Significance of Mississippian–Permian Granites in Zanskar

Previous studies have documented Cambrian–Ordovician granites in the Greater Himalayan Sequence related to the assembly of Gondwana (Yin and Harrison, 2000), and Miocene anatectic granites in the Greater Himalayan Sequence often have inherited Gondwanan zircon from 1700 to 800 Ma (Fig. 14; DeCelles et al., 2000). Previous Permian ages in Zanskar were correlated with the Swat granite gneiss in Pakistan (Noble et al., 2001; Spring et al., 1993), described by Kempe (1973), and dated by Anczkiewicz et al. (2001). Zircon cores of comparable age are reported farther north in the Kaghan valley, Pakistan (Wilke et al., 2010). Permian granites in Zanskar are ~10 m.y. older than adjacent Early to Middle Permian Panjal Trap flood basalts exposed west of Zanskar and near the Kaghan valley (Honegger et al., 1982; Chauvet et al., 2008, and references therein). Due to their alkaline composition, proximity to flood basalts, and approximately coeval ages, the Permian Zanskar granites have been described as extension-related melts caused by lithospheric thinning prior to the breakup of Gondwana and the formation of the Panjal Traps (Spring et al., 1993; Noble et al., 2001).

Lithosphere, published online on 20 April 2013 as doi:10.1130/L213.1

Evidence of Mississippian–Permian magmatism in the Greater Himalayan Sequence extends as far south as Mandi, near the Sutlej valley (Mehta, 1977), but not along the central and eastern portions of the Indian Himalaya. However, Zhu et al. (2009) obtained an average age of 262 Ma for granites near Pikang village in the southern Lhasa block. Whole-rock ICP-MS analyses on the Pikang granites show that they contain 70.5–73.6 wt% SiO_2, 1.51–2.03 K_2O/Na_2O, and have A/CNK [$Al_2O_3/(CaO + Na_2O + K_2O)$] values from 1.08 to 1.14, which correspond closely to whole-rock results for a 284 ± 1 Ma Zanskar granite with 72.2–75.2 wt% SiO_2, 0.7–3.3 K_2O/Na_2O, and A/CNK values of 1.1–1.24 (Spring et al., 1993). The Pikang granites have moderate $\varepsilon_{Hf}(t)$ values from –4.5 to +1.9, comparable to $\varepsilon_{Hf}(t)$ values for the ca. 285 Ma Zanskar granites, which range from –7.8 to +2.6. When plotted on a Zr-Y-Nb granite tectonic classification diagram published by Eby (1992), both the Pikang and Yunam granites appear related to continental rifting processes, while trace-element classification according to Pearce et al. (1984) suggests that the granites could be related to continental or oceanic subduction processes. The $\varepsilon_{Hf}(t)$ values for both the Zanskar and Pikang samples are lower than the Ladakh and Gangdese oceanic arcs ($\varepsilon_{Hf}[t]$ >2 for Cretaceous and older analyses; Chu et al., 2006; Wu et al., 2007), and much narrower than most inherited zircon populations from the Lhasa block (Chiu et al., 2009; Zhu et al., 2009) or Greater Himalayan Sequence. Based on this comparison, Permian granites in the eastern and western Himalaya are compositionally and isotopically similar and may be related to rifting processes associated with the breakup of Gondwana. This research suggests that Mississippian–Permian plutonism, while not as voluminous as Cambrian–Ordovician or Miocene granites, is geographically more extensive than previously documented. Because these Mississippian–Permian granites are isotopically and geochemically similar to granites in the Lhasa block, they may provide insight into the breakup of Gondwana and the paleo-juxtaposition of major Himalayan lithotectonic units.

CONCLUSIONS

Magmatism in the Karakoram shear zone began at or prior to ca. 22–21 Ma in Tangste gorge and continued until at least 13 Ma, and perhaps through 9 Ma (Figs. 6A–6F); distinct pulses of leucogranite crystallization at ca. 19 Ma and ca. 15 Ma may reflect periods of transpressional fault motion, as proposed by Weinberg et al. (2009). Results presented here support the hypothesis that the Karakoram shear zone has been a long-lived crustal-scale fault (e.g., Lacassin et al., 2004; Valli et al., 2007; Leloup et al., 2011; Klemperer et al., 2013).

Karakoram shear zone leucogranites have a predominantly positive $\varepsilon_{Hf}(t)$ signature that indicates they were mostly derived from source rock with recent mantle input; the Ladakh batholith seems the most probable candidate, considering chemical and isotopic similarities to Karakoram shear zone leucogranites (Weinberg and Dunlap, 2000; Reichardt et al., 2010). Input from older crustal sources such as the Karakoram terrane or subducted Indian crust could explain anomalously low $\varepsilon_{Hf}(t)$ values and pre-Cretaceous ages reported in this study and by Ravikant et al. (2009), but a lack of data from the Karakoram terrane and the isotopic heterogeneity of the Greater Himalayan Sequence prevent distinguishing between these two potential sources. Although this study does not exclude the possibility of input from a midcrustal channel, as proposed by Leech (2008), the age and isotopic characteristics of Karakoram shear zone granites can be explained by melt generation from local lithologies.

Partial melting and exhumation of the Greater Himalayan Sequence occurred contemporaneously across the Himalayan orogen (this study; Noble and Searle, 1995). Leucogranite magmatism in Haptal Tokpo occurred at ca. 27–20 Ma, and monazite ages range from 27 to 17 Ma, recording peak through retrograde metamorphic conditions. Unlike elsewhere in the Himalaya, the Greater Himalayan Sequence exposed in Zanskar did not undergo widespread anatectic melting in the Cenozoic, and doming plays a larger role in exhumation than elsewhere in the Himalaya (Kundig, 1989; Robyr et al., 2002). Abundant mica-poor Paleozoic granites may have created infertile zones of partial melting (Dézes et al., 1999), and erosion rates in Zanskar may have been too low to drive rapid exhumation by a standard channel flow model (Robyr et al., 2002). With similar lithologies and structures as the eastern Himalaya, but with the Karakoram fault limiting the northward subduction of Indian crust (Klemperer et al., 2013), Zanskar provides an ideal area to further test and constrain numerical channel flow models.

Zanskar geochronology presented here indicates that Mississippian–Permian granites are more extensive in the western Greater Himalayan Sequence than previously documented; ages, Hf isotopes, and geochemistry suggest that these granites may have formed in a similar tectonic setting as Permian granites to the west in Pakistan (e.g., Swat; Anczkiewicz et al., 2001) and to the east in the Lhasa block (e.g., Pikang; Zhu et al., 2009). We interpret the Mississippian–Permian granites as precursors to the Permian Panjal Traps flood basalts that erupted during the breakup of Gondwana.

APPENDIX A: METHODS

Minerals were separated at Stanford University using jaw-crushing, disc-mill, vibratory Gemini table, magnetic Frantz, and lithium metatungstate and methylene iodide heavy liquid techniques. No morphologic or color differentiation was made during handpicking for the sample mount. Zircons and monazites were mounted in four 25 mm cylindrical Struers EpoFix epoxy mounts, which were polished down to half-sections of grains using 6 µm and 1 µm diamond suspensions. Cathodoluminescence (CL) images were obtained on a W-filament JEOL 5600 LV scanning electron microscope with a Hamamatsu photo multiplier tube after being coated with gold. CL images were used to target specific growth zones and to avoid cracks and inclusions. To assess monazite growth conditions, several grains were scanned with a Cameca SX-100 Electron Probe Micro-Analyzer for La, Nd, Th, U, and Y using a 15 kV beam and 1 µm steps at the University of California at Santa Barbara.

In the SHRIMP, minerals were ablated with an O_2^- primary ion beam ranging from 3 to 6 nA, creating an ablation pit ~20 µm in diameter and <5 µm deep. For zircon analyses, peaks were measured sequentially for secondary ions $^{180}Zr_2{}^{16}O$, ^{204}Pb, ^{206}Pb, ^{207}Pb, ^{208}Pb, ^{232}Th, ^{238}U, $^{232}Th^{16}O$, $^{238}U^{16}O$, $^{238}U^{32}O_2$, and background. Zircon trace elements and Hf were collected immediately after for ^{89}Y, ^{139}La, ^{140}Ce, ^{146}Nd, ^{147}Sm, ^{153}Eu, ^{155}Gd, $^{163}Dy^{16}O$, $^{166}Er^{16}O$, ^{188}Yb, and $^{180}Hf^{16}O$. For monazite analyses, peaks were recorded for $^{140}Ce^{31}P^{32}O_2$, $^{232}Th^{143}Nd^{32}O_2$, ^{204}Pb, ^{206}Pb, ^{207}Pb, ^{208}Pb, ^{232}Th, ^{238}U, $^{232}Th^{16}O$, $^{238}U^{16}O$, $^{238}U^{32}O_2$, and background. Collection times varied from 1 to 25 s and were repeated four times for each peak. To avoid interference by other atomic species, measurements were made at mass resolutions 6000–8000 and 10% peak height. Zircon U concentrations were calculated using zircon standard MAD 4.6 (Madagascar green zircon with a known 4196 ppm U), and ages were corrected to zircon standard R33 with an age of 419 Ma (Black et al., 2004). Zircon data were reduced according to methods described in Williams (1998), using Microsoft Excel® Squid and Isoplot plugins (Ludwig, 2001, 2003). Trace-element concentrations were normalized to chondrite values of McDonough and Sun (1995). Monazite data were processed manually: Isotopic counts per second (cps) were divided by $^{140}Ce^{31}P^{32}O_2$ cps to calculate concentrations, and isotopic ratios were normalized to monazite standard 44069 with a U-Pb isotope dilution thermal ionization mass spectrometry age of 424.9 ± 0.4 Ma (Aleinikoff et al., 2006). Uncertainties associated with 44069 and experimental variances were propagated to calculate 1σ monazite age uncertainties.

LA-ICP-MS analyses were done according to the methods described by Gehrels et al. (2008) on a multicollector ICP-MS attached to a New Wave Instruments 193 nm ArF laser ablation system. For U-Pb analyses and then for Lu-Hf analyses, zircons were ablated by a beam with a 20 µm diameter, repetition rate of 8 Hz, and fluence of 4 J/cm^2, creating a pit 20–30 µm in depth. For U-Pb analyses, Faraday collectors with 3 × 10^{11} ohm resistors collected ^{238}U, ^{232}Th, ^{208}Pb, ^{207}Pb, and ^{206}Pb with 15 s backgrounds and peaks, while discrete dynode ion counters collected ^{204}Pb and ^{202}Pb with 15–12–10 s backgrounds and peaks. Sri Lanka zircon standard (SL; 563 ± 2.3 Ma) was analyzed once for every five unknown analyses. After corrections for background, down-hole fractionation, and $^{206}Pb/^{238}U$ fractionation were made as described by Gehrels et al. (2008), U-Pb ages were calculated according to Ludwig (2003) using the Arizona LaserChron NUcalc202 Microsoft Excel® plugin, and plotted with Isoplot. Spot analyses were discarded if ^{204}Pb > 300 cps, $^{206}Pb/^{238}U$ or $^{206}Pb/^{207}Pb$ ages were >10%, or if analyses were discordant by >30%.

For LA-ICP-MS Lu-Hf isotopic analysis, faradays were aligned to measure ^{180}Hf, ^{179}Hf, ^{178}Hf, ^{177}Hf, $^{176}(Hf,Lu,Yb)$, ^{175}Lu, ^{174}Hf, ^{173}Yb, ^{172}Yb, and ^{171}Yb. Each spot analysis included a 60 s background, followed by three blocks of 20 s measurements with 20 s of background in between. Zircon standards 91500, FC-52, Mud Tank, Temora-2, Plesovice, R33, and Sri Lanka-2 were analyzed every five unknown analyses and compared to solution ICP-MS results produced by Woodhead and Hergt (2005) and Sláma et al. (2008). Isotope fractionation of Hf was accounted for using the known constant $^{179}Hf/^{177}Hf$ ratio of 0.73250 (Patchett and Tatsumoto, 1981). Fractionation of

Yb was calculated assuming the constant $^{173}Yb/^{171}Yb$ ratio of 1.132338 (Vervoort, 2004), and the mass bias of Lu was assumed to behave the same as Yb. Interference of ^{176}Lu and ^{176}Yb was corrected using ^{175}Lu and ^{171}Yb measurements, respectively, and a 95% filter discarded the highest $^{176}Hf/^{177}Hf$ values. The ^{176}Lu decay constant of 1.867×10^{-11} (Scherer et al., 2001) and $^{206}Pb/^{238}U$ ages from each spot were used to calculate $^{176}Hf/^{177}Hf$ (T) values, which were normalized to the chondritic uniform reservoir (CHUR) for $\varepsilon_{Hf}(t)$ values. Lu-Hf data were processed with Microsoft Excel® plugin HfCalc_New, last updated by George Gehrels on 27 April 2010.

ACKNOWLEDGMENTS

This research was funded by a National Science Foundation (NSF) CAREER grant (EAR-0847721 to M.L. Leech) jointly supported by the Tectonics, Petrology & Geochemistry, and Education & Human Resources programs, an NSF Graduate Research Fellowship to F. Horton, and support from the Arizona LaserChron Center. William Hassett and John Sommerfeld provided advice and assistance throughout this study. Thanks go to Marty Grove and Joe Wooden for support in the Stanford–U.S. Geological Survey sensitive high-resolution ion microprobe (SHRIMP) laboratory, and to Trevor Dumitru for assistance with mineral separation. We also thank Stanzin Tharchen for support in Zanskar. Suggestions from Philippe Hervé Leloup, Stéphane Guillot, and one anonymous reviewer helped to improve an earlier version of this manuscript.

REFERENCES CITED

Aleinikoff, J.N., Schenck, W.S., Srogi, L., Fanning, C.M., Kamo, S.L., and Bosbyshell, H., 2006, Deciphering igneous and metamorphic events in high-grade rocks of the Wilmington Complex, Delaware: Morphology, cathodoluminescence and backscatter electron zoning, and SHRIMP U-Pb geochronology of zircon and monazite: Geological Society of America Bulletin, v. 118, p. 39–64, doi:10.1130/B25659.1.

Anczkiewicz, R., Oberli, F., Burg, J.P., Villa, I.M., Gunther, D., and Meier, M., 2001, Timing of normal faulting along the Indus suture in Pakistan Himalaya and a case of major $^{231}Pa/^{235}U$ initial disequilibrium in zircon: Earth and Planetary Science Letters, v. 191, p. 101–114, doi:10.1016/S0012-821X(01)00406-X.

Arora, B.R., Unsworth, M.J., and Rawat, G., 2007, Deep resistivity structure of the northwest Indian Himalaya and its tectonic implications: Geophysical Research Letters, v. 34, L04307, doi:10.1029/2006GL029165.

Barth, A.P., and Wooden, J.L., 2010, Coupled elemental and isotopic analyses of polygenetic zircons from granitic rocks by ion microprobe, with implications for melt evolution and the sources of granitic magmas: Chemical Geology, v. 277, p. 149–159, doi:10.1016/j.chemgeo.2010.07.017.

Beaumont, C., Jamieson, R.A., Nguyen, M.H., and Lee, B., 2001, Himalayan tectonics explained by extrusion of a low-viscosity crustal channel coupled to focused surface denudation: Nature, v. 414, p. 738–742, doi:10.1038/414738a.

Beaumont, C., Jamieson, R.A., Nguyen, M.H., and Medvedev, S., 2004, Crustal channel flows: Numerical models with applications to the tectonics of the Himalayan-Tibetan orogen: Journal of Geophysical Research, v. 109, B06406, doi:10.1029/2003JB002809.

Bhutani, R., Pande, K., and Desai, N., 2003, Age of the Karakoram fault activation: ^{40}Ar-^{39}Ar geochronological study of the Shyok suture zone in northern Ladakh, India: Current Science, v. 84, p. 1454–1458.

Black, L.P., Kamo, S., Allen, C.M., Davis, D.W., Aleinikoff, J.N., Valley, J.W., Mundil, R., Campbell, I.H., Korsch, R.J., Williams, S.I., and Foudoulis, C., 2004, Improved $^{206}Pb/^{238}U$ microprobe geochronology by the monitoring of a trace-element–related matrix effect; SHRIMP, ID-TIMS, ELA-ICP-MS and oxygen isotope documentation for a series of zircon standards: Chemical Geology, v. 205, p. 115–140, doi:10.1016/j.chemgeo.2004.01.003.

Bouilhol, P., Jagoutz, O., and Hanchar, J.M., 2010a, The change of source composition in plutonic rocks from the Kohistan-Ladakh arc constrain the onset of collision along the Indus suture in the western Himalaya: Geological Society of America Abstracts with Programs, v. 42, no. 5, p. 664.

Bouilhol, P., Schaltegger, U., Chiaradia, M., Ovtcharova, M., Stracke, A., Burg, J.P., and Dawood, H., 2010b, Timing of juvenile arc crust formation and evolution in the Sapat Complex (Kohistan-Pakistan): Chemical Geology, v. 280, p. 243–256, doi:10.1016/j.chemgeo.2010.11.013.

Boutonnet, E., Leloup, P.H., Arnaud, N., Paquette, J.-L., Davis, W.J., and Hattori, K., 2012, Synkinematic magmatism, heterogeneous deformation, and progressive strain localization in a strike-slip shear zone: The case of the right-lateral Karakorum fault: Tectonics, v. 31, TC4012, doi:10.1029/2011TC003049.

Brown, E.T., Molnar, P., and Bourlès, D.L., 2005, Slip-rate measurements on the Karakorum fault may imply secular variations in fault motion: Science, v. 309, p. 1326, doi:10.1126/science.1112508.

Caldwell, W.B., Klemperer, S.L., Rai, S.S., and Lawrence, J.F., 2009, Partial melt in the upper-middle crust of the northwest Himalaya revealed by Rayleigh wave dispersion: Tectonophysics, v. 477, p. 58–65, doi:10.1016/j.tecto.2009.01.013.

Castiñeiras, P., García, F.D., and Barreiro, J.G., 2010, REE-assisted U-Pb zircon age (SHRIMP) of an anatectic granodiorite: Constraints on the evolution of the A Silva granodiorite, Iberian allochthonous complexes: Lithos, v. 116, p. 153–166, doi:10.1016/j.lithos.2010.01.013.

Chauvet, F., Lapierre, H., Bosch, D., Guillot, S., Mascle, G., Vannay, J.C., Cotten, J., Brunet, P., and Keller, F., 2008, Geochemistry of the Panjal Traps basalts (NW Himalaya): Records of the Pangea Permian break-up: Bulletin de la Société Géologique de France, v. 179, p. 383–395, doi:10.2113/gssgfbull.179.4.383.

Chevalier, M., Ryerson, F.J., Tapponnier, P., Finkel, R.C., Van Der Woerd, J., Haibing, L., and Qing, L., 2005a, Slip-rate measurements on the Karakorum fault may imply secular variations in fault motion: Science, v. 307, p. 411–414, doi:10.1126/science.1105466.

Chevalier, M., Ryerson, F.J., Tapponnier, P., Finkel, R.C., Van Der Woerd, J., Haibing, L., and Qing, L., 2005b, Response to Comment on "Slip-rate measurements on the Karakorum fault may imply secular variations in fault motion": Science, v. 309, p. 1326c, doi:10.1126/science.1112629.

Chiu, H.Y., Chung, S.L., Wu, F.Y., Liu, D., Liang, Y.H., Lin, I.J., Iizuka, Y., Xie, L.W., Wang, Y., and Chu, M.F., 2009, Zircon U-Pb and Hf isotopic constraints from eastern Transhimalayan batholiths on the precollisional magmatic and tectonic evolution in southern Tibet: Tectonophysics, v. 477, p. 3–19, doi:10.1016/j.tecto.2009.02.034.

Chu, M.F., Chung, S.L., Song, B., Liu, D., O'Reilly, S.Y., Pearson, N.J., Ji, J., and Wen, D.J., 2006, Zircon U-Pb and Hf isotope constraints on the Mesozoic tectonics and crustal evolution of southern Tibet: Geology, v. 34, p. 745–748, doi:10.1130/G22725.1.

Condie, K.C., Beyer, E., Belousova, E., Griffin, W.L., and O'Reilly, S.Y., 2005, U-Pb isotopic ages and Hf isotopic composition of single zircons: The search for juvenile Precambrian continental crust: Precambrian Research, v. 139, p. 42–100, doi:10.1016/j.precamres.2005.04.006.

DeCelles, P.G., Gehrels, G.E., Quade, J., LaReau, B., and Spurlin, M., 2000, Tectonic implications of U-Pb zircon ages of the Himalayan orogenic belt in Nepal: Science, v. 288, p. 497, doi:10.1126/science.288.5465.497.

Dézes, P.J., Vannay, J.-C., Steck, A., and Bussy, F., 1999, Synorogenic extension: Quantitative constraints on the age and displacement of the Zanskar shear zone (northwest Himalaya): Geological Society of America Bulletin, v. 111, p. 364–374, doi:10.1130/0016-7606(1999)111<0364:SEQCOT>2.3.CO;2.

Dunlap, W.J., and Wysoczanski, R., 2002, Thermal evidence for Early Cretaceous metamorphism in the Shyok suture zone and age of the Khardung volcanic rocks, Ladakh, India: Journal of Asian Earth Sciences, v. 20, p. 481–490, doi:10.1016/S1367-9120(01)00042-6.

Eby, G.N., 1992, Chemical subdivision of the A-type granitoids: Petrogenetic and tectonic implications: Geology, v. 20, p. 641–644, doi:10.1130/0091-7613(1992)020<0641:CSOTAT>2.3.CO;2.

Frank, W., Thoni, M., and Purtscheller, F., 1977, Geology and Petrography of Kulu–South Lahoul area: Colloque Internationale, Centre National de la Recherche Scientifique, Himalaya: Science de la Terra, v. 268, p. 147–166.

Fraser, J.E., Searle, M.P., Parrish, R.R., and Noble, S.R., 2001, Chronology of deformation, metamorphism, and magmatism in the southern Karakoram Mountains: Geological Society of America Bulletin, v. 113, p. 1443–1455, doi:10.1130/0016-7606(2001)113<1443:CODMAM>2.0.CO;2.

Gapais, D., Pecher, A., Gilbert, E., and Ballevre, M., 1992, Synconvergence spreading of the higher Himalaya crystalline in Ladakh: Tectonics, v. 11, p. 1045–1056, doi:10.1029/92TC00819.

Gehrels, G.E., 2010, Hf Analytical Methods at the Arizona LaserChron Center (University of Arizona): https://sites.google.com/a/laserchron.org/laserchron/home, updated 08/06/2010 (accessed February 2012).

Gehrels, G.E., Valencia, V., and Ruiz, J., 2008, Enhanced precision, accuracy, efficiency, and spatial resolution of U-Pb ages by laser ablation–multicollector–inductively coupled plasma–mass spectrometry: Geochemistry Geophysics Geosystems, v. 9, Q03017, doi:10.1029/2007GC001805.

Godin, L., Grujic, D., Law, R.D., and Searle, M.P., 2006, Channel flow, ductile extrusion and exhumation in continental collision zones: An introduction, *in* Law, R.D., Searle, M.P., and Godin, L., eds., Channel Flow, Ductile Extrusion and Exhumation in Continental Collision Zones: Geological Society of London Special Publication 268, p. 1–23, doi:10.1144/GSL.SP.2006.268.01.01.

Grujic, D., 2006, Channel flow and continental collision tectonics: An overview, *in* Law, R.D., Searle, M.P., and Godin, L., eds., Channel Flow, Ductile Extrusion and Exhumation in Continental Collision Zones: Geological Society of London Special Publication 268, p. 25–37, doi:10.1144/GSL.SP.2006.268.01.02.

Grujic, D., Hollister, L.S., and Parrish, R.P., 2002, Himalayan metamorphic sequence as an orogenic channel: Insight from Bhutan: Earth and Planetary Science Letters, v. 198, p. 177–191, doi:10.1016/S0012-821X(02)00482-X.

Herren, E., 1987a, The Zanskar shear zone: Northeast-southwest extension within the Higher Himalayas (Ladakh, India): Geology, v. 15, p. 409–413, doi:10.1130/0091-7613(1987)15<409:ZSZNEW>2.0.CO;2.

Herren, E., 1987b, Structures, Deformation and Metamorphism of the Zanskar Area (Ladakh, NW-Himalaya) [Ph.D. thesis]: Zurich, Switzerland, EHT Zurich, 147 p.

Herren, E., 1988, Discussion, *in* Searle, M.P., Cooper, D.J.W., Rex, A.J., Herren, E., Rex, A.J., and Colchen, M., 1988, Collision Tectonics of the Ladakh–Zanskar Himalaya [and Discussion]: Philosophical Transactions of the Royal Society of London, ser. A, Mathematical and Physical Sciences, v. 326, p. 117–150.

Heuberger, S., Schaltegger, U., Burg, J.-P., Villa, I.M., Frank, M., Dawood, H., Hussain, S., and Zanchi, A., 2007, Age and isotopic constraints on magmatism along the Karakoram-Kohistan suture zone, NW Pakistan: Evidence for subduction and continued convergence after India-Asia collision: Swiss Journal of Geosciences, v. 100, p. 85–107, doi:10.1007/s00015-007-1203-7.

Honegger, K., 1983, Strukturen und Metamorphose im Zanskar Kristallin [Ph.D. thesis]: Zurich, Switzerland, EHT Zurich, 117 p.

Honegger, K., Dietrich, V., Frank, W., Gansser, A., Thöni, M., and Trommsdorff, V., 1982, Magmatism and metamorphism in the Ladakh Himalayas (the Indus-Tsangpo suture zone): Earth and Planetary Science Letters, v. 60, p. 253–292, doi:10.1016/0012-821X(82)90007-3.

Inger, S., 1998, Timing of an extensional detachment during convergent orogeny: New Rb-Sr geochronological data from the Zanskar shear zone, northwestern Himalaya: Geology, v. 26, p. 223–226, doi:10.1130/0091-7613(1998)026<0223:TOAEDD>2.3.CO;2.

Jade, S., Bhatt, B.C., Yang, Z., Bendick, R., Gaur, V.K., Molnar, P., Anand, M.P., and Kumar, D., 2004, GPS measurements from the Ladakh Himalaya, India: Preliminary tests of plate-like or continuous deformation in Tibet: Geological Society of America Bulletin, v. 116, p. 1385–1391, doi:10.1130/B25357.1.

Jain, A.K., and Singh, S., 2008, Tectonics of the southern Asian plate margin along the Karakoram shear zone: Constraints from field observations and U-Pb SHRIMP ages: Tectonophysics, v. 451, p. 186–205, doi:10.1016/j.tecto.2007.11.048.

Ji, W.Q., Wu, F.Y., Chung, S.L., Li, J.X., and Liu, C.Z., 2009, Zircon U-Pb geochronology and Hf isotopic constraints on petrogenesis of the Gangdese batholith, southern Tibet: Chemical Geology, v. 262, p. 229–245, doi:10.1016/j.chemgeo.2009.01.020.

Kempe, D.R.C., 1973, The petrology of the Warsak alkaline granites, Pakistan, and their relationship to other alkaline rocks of the region: Geological Magazine, v. 110, p. 385–404, doi:10.1017/S0016756800036189.

Klemperer, S.L., Kennedy, B.M., Sastry, S.R., Makovsky, Y., Harinarayana, T., and Leech, M.L., 2013, Mantle fluids in the Karakoram fault: Helium isotope evidence: Earth and Planetary Science Letters, v. 366, p. 59–70, doi:10.1016/j.epsl.2013.01.013.

Kundig, R., 1989, Domal structures and high-grade metamorphism in the Higher Himalayan Crystalline, Zanskar region, northwest Himalaya, India: Journal of Metamorphic Geology, v. 7, p. 43–55, doi:10.1111/j.1525-1314.1989.tb00574.x.

Lacassin, R., Valli, F., Arnaud, N., Leloup, P.H., Paquette, J.L., Haibing, L., Tapponnier, P., Chevalier, M.L., Guillot, S., Maheo, G., et al., 2004, Large-scale geometry, offset and kinematic evolution of the Karakorum fault, Tibet: Earth and Planetary Science Letters, v. 219, p. 255–269, doi:10.1016/S0012-821X(04)00006-8.

Leech, M.L., 2008, Does the Karakoram fault interrupt midcrustal channel flow in the western Himalaya?: Earth and Planetary Science Letters, v. 276, p. 314–322, doi:10.1016/j.epsl.2008.10.006.

Leier, A.L., Kapp, P., Gehrels, G.E., and DeCelles, P.G., 2007, Detrital zircon geochronology of Carboniferous–Cretaceous strata in the Lhasa terrane, southern Tibet: Basin Research, v. 19, p. 361–378, doi:10.1111/j.1365-2117.2007.00330.x.

Leloup, P.H., Mahéo, G., Arnaud, N., Kali, E., Boutonnet, E., Liu, D., Xiaohan, L., and Haibing, L., 2010, The South Tibet detachment shear zone in the Dinggye area: Time constraints on extrusion models of the Himalayas: Earth and Planetary Science Letters, v. 292, p. 1–16, doi:10.1016/j.epsl.2009.12.035.

Leloup, P.H., Boutonnet, E., Davis, W.J., and Hattori, K., 2011, Long-lasting intracontinental strike-slip faulting: New evidence from the Karakorum shear zone in the Himalayas: Terra Nova, v. 23, p. 92–99.

Ludwig, K.R., 2001, Squid 1.02: A User's Manual: Berkeley Geochronology Center Special Publication 2, 22 p.

Ludwig, K.R., 2003, User's Manual for Isoplot 3.00: A Geochronological Toolkit for Microsoft Excel: Berkeley Geochronology Center Special Publication 4, 73 p.

Mahéo, G., Guillot, S., Blichert-Toft, J., Rolland, Y., and Pecher, A., 2002, A slab breakoff model for the Neogene thermal evolution of South Karakorum and South Tibet: Earth and Planetary Science Letters, v. 195, no. 1, p. 45–58, doi:10.1016/S0012-821X(01)00578-7.

Mahéo, G., Blichert-Toft, J., Pin, C., Guillot, S., and Pêcher, A., 2009, Partial melting of mantle and crustal sources beneath South Karakorum, Pakistan: Implications for the Miocene geodynamic evolution of the India–Asia convergence zone: Journal of Petrology, v. 50, no. 3, p. 427–449, doi:10.1093/petrology/egp006.

McDonough, W.F., and Sun, S., 1995, The composition of the Earth: Chemical Geology, v. 120, p. 223–253, doi:10.1016/0009-2541(94)00140-4.

Mehta, P.K., 1977, Rb-Sr geochronology of the Kulu-Mandi belt: Its implications for the Himalayan tectogenesis: Geologische Rundschau, v. 66, p. 156–175, doi:10.1007/BF01989570.

Murphy, M.A., Yin, A., Kapp, P., Harrison, T.M., and Manning, C.E., 2002, Structural evolution of the Gurla Mandhata detachment system, southwest Tibet: Implications for the eastward extent of the Karakoram fault system: Geological Society of America Bulletin, v. 114, p. 428–447, doi:10.1130/0016-7606(2002)114<0428:SEOTGM>2.0.CO;2.

Nelson, K.D., Zhao, W., Brown, L.D., Kuo, J., Che, J., Liu, X., Klemperer, S.L., Makovsky, Y., Meissner, R., Mechie, J., Kind, R., Wenzel, F., Ni, J., Nabelek, J., Leshou, C., Tan, H., Wei, W., Jones, A.G., Booker, J., Unsworth, M., Kidd, W.S.F., Hauck, M., Alsdorf, D., Ross, A., Cogan, M., Wu, C., Sandvol, E., and Edwards, M., 1996, Partially molten middle crust beneath southern Tibet: Synthesis of Project INDEPTH results: Science, v. 274, p. 1684–1688, doi:10.1126/science.274.5293.1684.

Noble, S.R., and Searle, M.P., 1995, Age of crustal melting and leucogranite formation from U-Pb zircon and monazite dating in the western Himalaya, Zanskar, India: Geology, v. 23, p. 1135–1138, doi:10.1130/0091-7613(1995)023<1135:AOCMAL>2.3.CO;2.

Noble, S.R., Searle, M.P., and Walker, C.B., 2001, Age and tectonic significance of Permian granites in western Zanskar, High Himalaya: The Journal of Geology, v. 109, p. 127–135, doi:10.1086/317966.

Parrish, R.R., 1990, U-Pb dating of monazite and its application to geological problems: Canadian Journal of Earth Sciences, v. 27, p. 1431–1450, doi:10.1139/e90-152.

Patchett, P.J., and Tatsumoto, M., 1981, A routine high-precision method for Lu-Hf isotope geochemistry and chronology: Contributions to Mineralogy and Petrology, v. 75, p. 263–267, doi:10.1007/BF01166766.

Pearce, J.A., Harris, N.B.W., and Tindle, A.G., 1984, Trace element discrimination diagrams for the tectonic interpretation of granitic rocks: Journal of Petrology, v. 25, p. 956–983, doi:10.1093/petrology/25.4.956.

Phillips, R.J., 2008, Geologic Map of the Karakoram Fault Zone, Eastern Karakoram, Ladakh, NW Himalaya: Journal of Maps, p. 21–37, doi: 10.4113/jom.2008.98.

Phillips, R.J., and Searle, M.P., 2007, Macrostructural and microstructural architecture of the Karakoram fault: Relationship between magmatism and strike-slip faulting: Tectonics, v. 26, TC3017, doi:10.1029/2006TC001946.

Phillips, R.J., Parrish, R.R., and Searle, M.P., 2004, Age constraints on ductile deformation and long-term slip rates along the Karakoram fault zone, Ladakh: Earth and Planetary Science Letters, v. 226, p. 305–319, doi:10.1016/j.epsl.2004.07.037.

Pognante, U., 1992, Migmatites and leucogranites of Tertiary age from the High Himalayan Crystallines of Zanskar (NW India): A case history of anatexis of Palaeozoic orthogneisses: Mineralogy and Petrology, v. 46, p. 291–313, doi:10.1007/BF01173569.

Pognante, U., Castelli, D., Benna, P., Genovese, G., Oberli, F., Meier, M., and Tonarini, S., 1990, The crystalline units of the High Himalayas in the Lahul–Zanskar region (northwest India): Metamorphic–tectonic history and geochronology of the collided and imbricated Indian plate: Geological Magazine, v. 127, p. 101–116, doi:10.1017/S0016756800013807.

Pyle, J.M., and Spear, F.S., 2003, Four generations of accessory-phase growth in low-pressure migmatites from SW New Hampshire: The American Mineralogist, v. 88, p. 338–351.

Ravikant, V., 2006, Utility of Rb-Sr geochronology in constraining Miocene and Cretaceous events in the eastern Karakoram, Ladakh, India: Journal of Asian Earth Sciences, v. 27, p. 534–543, doi:10.1016/j.jseaes.2005.05.007.

Ravikant, V., Wu, F., and Ji, W., 2009, Zircon U-Pb and Hf isotopic constraints on petrogenesis of the Cretaceous-Tertiary granites in eastern Karakoram and Ladakh, India: Lithos, v. 110, p. 153–166, doi:10.1016/j.lithos.2008.12.013.

Reichardt, H., Weinberg, R.F., Andersson, U.B., and Fanning, C.M., 2010, Hybridization of granitic magmas in the source: The origin of the Karakoram Batholith, Ladakh, NW India: Lithos, v. 116, p. 249–272, doi:10.1016/j.lithos.2009.11.013.

Rex, A.J., Searle, M.P., Tirrul, R., Crawford, M.B., Prior, D.J., Rex, D.C., Barnicoat, A., and Bertrand, J.-M., 1988, The geochemical and tectonic evolution of the central Karakoram, north Pakistan: Philosophical Transactions of the Royal Society of London, ser. A, Mathematical and Physical Sciences, v. 326, p. 229–255.

Richards, A., Argles, T., Harris, N., Parrish, R., Ahmad, T., Darbyshire, F., and Draganits, E., 2005, Himalayan architecture constrained by isotopic tracers from clastic sediments: Earth and Planetary Science Letters, v. 236, p. 773–796, doi:10.1016/j.epsl.2005.05.034.

Robyr, M., Vannay, J.C., Epard, J.L., and Steck, A., 2002, Thrusting, extension, and doming during the polyphase tectonometamorphic evolution of the High Himalayan Crystalline Zone in NW India: Journal of Asian Earth Sciences, v. 21, p. 221–239, doi:10.1016/S1367-9120(02)00039-1.

Robyr, M., Hacker, B.R., and Mattinson, J.M., 2006, Doming in compressional orogenic settings: New geochronological constraints from the NW Himalaya: Tectonics, v. 25, p. TC2007, doi:10.1029/2004TC001774.

Rolland, Y., and Pêcher, A., 2001, The Pangong granulites of the Karakoram fault (western Tibet): Vertical extrusion within a lithosphere-scale fault?: Comptes Rendus de l'Académie des Sciences, ser. IIA, Earth and Planetary Science, v. 332, p. 363–370.

Rosenberg, C.L., and Handy, M.R., 2005, Experimental deformation of partially melted granite revisited: Implications for the continental crust: Journal of Metamorphic Geology, v. 23, p. 19–28.

Rubatto, D., Williams, I.S., and Buick, I.S., 2001, Zircon and monazite response to prograde metamorphism in the Reynolds Range, central Australia: Contributions to Mineralogy and Petrology, v. 140, p. 458–468, doi:10.1007/PL00007673.

Rutter, E.H., Faulkner, D.R., Brodie, K.H., Phillips, R.J., and Searle, M.P., 2007, Rock deformation processes in the Karakoram fault zone, Eastern Karakoram, Ladakh, NW India: Journal of Structural Geology, v. 29, p. 1315–1326, doi:10.1016/j.jsg.2007.05.001.

Schaltegger, U., Zeilinger, G., Frank, M., and Burg, J.P., 2002, Multiple mantle sources during island arc magmatism: U-Pb and Hf isotopic evidence from the Kohistan arc complex, Pakistan: Terra Nova, v. 14, p. 461–468, doi:10.1046/j.1365-3121.2002.00432.x.

Schärer, U., 1984, The effect of initial ^{230}Th disequilibrium on young U-Pb ages: The Makalu case, Himalaya: Earth and Planetary Science Letters, v. 67, no. 2, p. 191–204, doi:10.1016/0012-821X(84)90114-6.

Schärer, U., Copeland, P., Harrison, T.M., and Searle, M.P., 1990, Age, cooling history, and origin of post-collisional leucogranites in the Karakoram Batholith: A multisystem isotope study: The Journal of Geology, v. 98, p. 233–251, doi:10.1086/629395.

Scherer, E., Munker, C., and Mezger, K., 2001, Calibration of the lutetium-hafnium clock: Science, v. 293, p. 683–687, doi:10.1126/science.1061372.

Searle, M.P., 1986, Structural evolution and sequence of thrusting in the High Himalayan, Tibetan–Tethys and Indus suture zones of Zanskar and Ladakh, western Himalaya: Journal of Structural Geology, v. 8, p. 923–936, doi:10.1016/0191-8141(86)90037-4.

Searle, M.P., and Fryer, B.J., 1986, Garnet, tourmaline and muscovite-bearing leucogranites, gneisses and migmatites of the Higher Himalayas from Zanskar, Kulu, Lahoul and Kashmir, *in* Coward, M.P., and Ries, A.C., eds., Collision Tectonics: Geological Society of London Special Publication 19, p. 185–201, doi:10.1144/GSL.SP.1986.019.01.10.

Searle, M.P., and Phillips, R.J., 2007, Relationships between right-lateral shear along the Karakoram fault and metamorphism, magmatism, exhumation and uplift: Evidence from the K2-Gasherbrum-Pangong ranges, north Pakistan and Ladakh: Journal of the Geological Society of London, v. 164, p. 439–450, doi:10.1144/0016"-76492006-072.

Searle, M.P., and Rex, A.J., 1989, Thermal model for the Zanskar Himalaya: Journal of Metamorphic Geology, v. 7, p. 127–134, doi:10.1111/j.1525-1314.1989.tb00579.x.

Searle, M.P., Waters, D.J., Rex, D.C., and Wilson, R.N., 1992, Pressure, temperature and time constraints on Himalayan metamorphism from eastern Kashmir and western Zanskar: Journal of the Geological Society of London, v. 149, p. 753–773, doi:10.1144/gsjgs.149.5.0753.

Searle, M.P., Weinberg, R.F., and Dunlap, W.J., 1998, Transpressional tectonics along the Karakoram fault zone, northern Ladakh: Constraints on Tibetan extrusion, *in* Holdsworth, R.E., Strachan, R.A., and Dewey, J.F., eds., Continental Transpressional and Transtensional Tectonics: Geological Society of London Special Publication 135, p. 307–326, doi:10.1144/GSL.SP.1998.135.01.20.

Searle, M.P., Waters, D.J., Dransfield, M.W., Stephenson, B.J., Walker, C.B., Walker, J.D., and Rex, D.C., 1999, Thermal and mechanical models for the structural and metamorphic evolution of the Zanskar High Himalaya, *in* Mac Niocaill, C., and Ryan P.D., eds., Continental Tectonics: Geological Society of London Special Publication 164, p. 139–156, doi:10.1144/GSL.SP.1999.164.01.08.

Sláma, J., Kosler, J., Condon, D.J., Crowley, J.L., Gerdes, A., Hanchar, J.M., Horstwood, M.S., Morris, G.A., Nasdala, L., Norberg, N., Schaltegger, U., Schoene, B., Tubrett, M.N., and Whitehouse, M.J., 2008, Plesovice zircon—A new natural reference material for U-Pb and Hf isotopic microanalysis: Chemical Geology, v. 249, p. 1–35, doi:10.1016/j.chemgeo.2007.11.005.

Spear, F.S., and Pyle, J.M., 2002, Apatite, monazite, and xenotime in metamorphic rocks: Reviews in Mineral-

ogy and Geochemistry, v. 48, p. 293–335, doi:10.2138/rmg.2002.48.7.

Spring, L., Bussy, F., Vannay, J.C., Huon, S., and Cosca, M.A., 1993, Early Permian granitic dykes of alkaline affinity in the Indian High Himalaya of Upper Lahul and SE Zanskar: Geochemical characterization and geotectonic implications, *in* Treloar, P.J., and Searle M.P., eds., Himalayan Tectonics: Geological Society of London Special Publication 74, p. 251–264, doi:10.1144/GSL.SP.1993.074.01.18.

Steck, A., 2003, Geology of the NW Indian Himalaya: Eclogae Geologicae Helvetiae, v. 96, p. 147–196.

Stutz, E., and Thöni, M., 1987, The lower Paleozoic Nyimaling Granite in the Indian Himalaya (Ladakh): New Rb/Sr data versus zircon typology: Geologische Rundschau, v. 76, p. 307–315, doi:10.1007/BF01821076.

Unsworth, M.J., Jones, A.G., Wei, W., Marquis, G., Gokarn, S.G., and Spratt, J.E., 2005, Crustal rheology of the Himalaya and southern Tibet inferred from magnetotelluric data: Nature, v. 438, p. 78–81, doi:10.1038/nature04154.

Valli, F., Arnaud, N., Leloup, P.H., Sobel, E.R., Maheo, G., Lacassin, R., Guillot, S., Le, H., Tapponnier, P., and Xu, Z., 2007, Twenty million years of continuous deformation along the Karakoram fault, western Tibet: A thermochronological analysis: Tectonics, v. 26, TC4004, doi:10.1029/2005TC001913.

Valli, F., Leloup, P.H., Paquette, J.L., Arnaud, N., Li, H., Tapponnier, P., Lacassin, R., Guillot, S., Liu, D., and Deloule, E., 2008, New U-Th/Pb constraints on timing of shearing and long-term slip-rate on the Karakorum fault: Tectonics, v. 27, no. 5, TC5007, doi:10.1029/2007TC002184.

Vance, D., and Harris, N., 1999, Timing of prograde metamorphism in the Zanskar Himalaya: Geology, v. 27, p. 395–398, doi:10.1130/0091-7613(1999)027<0395:TOPMIT>2.3.CO;2.

Vervoort, J.D., 2004, Isotopic composition of Yb and the determination of Lu concentrations and Lu/Hf ratios by isotope dilution using MC-ICPMS: Geochemistry Geophysics Geosystems, v. 5, Q11002, doi:10.1029/2004GC000721.

Walker, C.B., Searle, M.P., and Waters, D.J., 2001, An integrated tectonothermal model for the evolution of the High Himalaya in western Zanskar with constraints from thermobarometry and metamorphic modeling: Tectonics, v. 20, p. 810–833, doi:10.1029/2000TC001249.

Walker, J.D., Martin, M.W., Bowring, S.A., Searle, M.P., Waters, D.J., and Hodges, K.V., 1999, Metamorphism, melting, and extension: Age constraints from the High Himalayan slab of southeast Zanskar and northwest Lahaul: The Journal of Geology, v. 107, p. 473–495, doi:10.1086/314360.

Wang, S., Wang, C., Phillips, R.J., Murphy, M.A., Fang, X., and Yue, Y., 2012, Displacement along the Karakoram fault, NW Himalaya, estimated from LA-ICP-MS U-Pb dating of offset geologic markers: Earth and Planetary Science Letters, v. 337–338, p. 156–163, doi:10.1016/j.epsl.2012.05.037.

Weinberg, R.F., and Dunlap, W.J., 2000, Growth and deformation of the Ladakh Batholith, northwest Himalayas: Implications for timing of continental collision and origin of calc-alkaline batholiths: The Journal of Geology, v. 108, p. 303–320, doi:10.1086/314405.

Weinberg, R.F., and Mark, G., 2008, Magma migration, folding, and disaggregation of migmatites in the Karakoram shear zone, Ladakh, NW India: Geological Society of America Bulletin, v. 120, p. 994–1009, doi:10.1130/B26227.1.

Weinberg, R.F., Mark, G., and Reichardt, H., 2009, Magma ponding in the Karakoram shear zone, Ladakh, NW India: Geological Society of America Bulletin, v. 121, p. 278–285.

Whipple, K.X., 2009, The influence of climate on the tectonic evolution of mountain belts: Nature Geoscience, v. 2, p. 97–104, doi:10.1038/ngeo413.

Whitney, D.L., and Evans, B.W., 2010, Abbreviations for names of rock-forming minerals: American Mineralogist, v. 95, p. 185–187, doi:10.2138/am.2010.3371

Whittington, A., Harris, N.B.W., Ayres, M.W., and Foster, G., 2000, Tracing the origins of the western Himalaya: An isotopic comparison of the Nanga Parbat massif and Zanskar Himalaya, *in* Asif Khan, M., Treloar, P.J., Searle, M.P., and Qasim Jan, M., eds., Tectonics of the Nanga Parbat Syntaxis and the Western Himalaya: Geological Society of London Special Publication 170, p. 201–218, doi:10.1144/GSL.SP.2000.170.01.11.

Wilke, F.D.H., O'Brien, P.J., Gerdes, A., Timmerman, M.J., Sudo, M., and Ahmed, K., 2010, The multistage exhumation history of the Kaghan valley UHP series, NW Himalaya, Pakistan, from U-Pb and $^{40}Ar/^{39}Ar$ ages: European Journal of Mineralogy, v. 22, p. 703–719, doi:10.1127/0935-1221/2010/0022-2051.

Williams, I.S., 1998, U-Th-Pb geochronology by ion microprobe, *in* McKibben, M.A., Shanks, W.C., III, and Ridley, W.I., eds., Applications of Microanalytical Techniques to Understanding Mineralizing Processes: Society of Economic Geologists, Reviews in Economic Geology, v. 7, p. 1–35.

Williams, M.L., Jercinovic, M.J., Harlov, D.E., Budzyń, B., and Hetherington, C.J., 2011, Resetting monazite ages during fluid-related alteration: Chemical Geology, v. 283, p. 218–225, doi:10.1016/j.chemgeo.2011.01.019.

Woodhead, J.D., and Hergt, J.M., 2005, A preliminary appraisal of seven natural zircon reference materials for in situ Hf isotope determination: Geostandards and Geoanalytical Research, v. 29, p. 183–195, doi:10.1111/j.1751-908X.2005.tb00891.x.

Wu, F., Clift, P.D., and Yang, J., 2007, Zircon Hf isotopic constraints on the sources of the Indus Molasse, Ladakh Himalaya, India: Tectonics, v. 26, TC2014, doi:10.1029/2006TC002051.

Yin, A., and Harrison, T.M., 2000, Geologic evolution of the Himalayan Tibetan orogen: Annual Review of Earth and Planetary Sciences, v. 28, p. 211–280, doi:10.1146/annurev.earth.28.1.211.

Zhu, D.C., Mo, X.X., Niu, Y., Zhao, Z.D., Wang, L.Q., Pan, G.T., and Wu, F.Y., 2009, Zircon U-Pb dating and in-situ Hf isotopic analysis of Permian peraluminous granite in the Lhasa terrane, southern Tibet: Implications for Permian collisional orogeny and paleogeography: Tectonophysics, v. 469, p. 48–60, doi:10.1016/j.tecto.2009.01.017.

Zhu, X., and O'Nions, R., 1999, Zonation of monazite in metamorphic rocks and its implications for high temperature thermochronology: A case study from the Lewisian terrain: Earth and Planetary Science Letters, v. 171, p. 209–220, doi:10.1016/S0012-821X(99)00146-6.

MANUSCRIPT RECEIVED 20 MARCH 2012
REVISED MANUSCRIPT RECEIVED 20 FEBRUARY 2013
MANUSCRIPT ACCEPTED 3 MARCH 2013

Printed in the USA